Marine and Petroleum Geology 142 (2022) 105738

Contents lists available at ScienceDirect

Marine and Petroleum Geology

journal homepage: www.elsevier.com/locate/marpetgeo

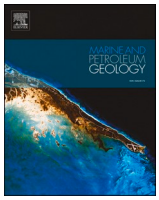

The nature, origin, and predictors of porosity in the Middle to Late Devonian Horn River Group of the Central Mackenzie Valley, Northwest Territories, Canada

Maya T. LaGrange [a,*], Nicole Mae M. Atienza [a], Sara K. Biddle [a], Brette S. Harris [a], Kathryn M. Fiess [b], Viktor Terlaky [b], Kurt O. Konhauser [a], Murray K. Gingras [a]

[a] Department of Earth and Atmospheric Sciences, University of Alberta, Edmonton, Alberta, T6G 2E3, Canada
[b] Northwest Territories Geological Survey, Government of Northwest Territories, P.O. Box 1320, 4601-B 52nd Ave, Yellowknife, Northwest Territories, X1A 2L9, Canada

ARTICLE INFO

Keywords:
Porosity
Black shale
Organic-rich mudstone
Canol Formation
Horn River Group

ABSTRACT

The characterization of porosity is an essential step in the evaluation of resource-bearing porous media. Here, we focus on the Devonian Hare Indian and Canol Formations, two potential unconventional mudstone reservoirs, in a core from the Horn River Group of the Central Mackenzie Valley, Northwest Territories, Canada. By combining bulk porosity, low-pressure N_2 adsorption, and scanning electron microscopy (SEM) results with composition and lithofacies datasets, we assess the porosity in these successions to understand pore types, size, distribution, degree of connectivity, and controls and predictors of porosity. Mineral matrix pores (interparticle and intraparticle), organic matter pores, and lithofacies-dependant natural fractures are present. All pore types display limited connectivity in two dimensions. Mineralogy is the most significant control on porosity with trends in porosity present among lithofacies. No relationship is observed between porosity and total organic carbon (TOC), suggesting that mineral matrix pores, rather than organic matter pores, are dominant in this unit. We compare these results to other mudstone reservoirs in North America and show that the Bluefish Member (Hare Indian Formation) and the Canol Formation are characterized by comparable bulk porosity, lower N_2 mesopore volume, and higher quartz content relative to the other units considered. In contrast, compared to the other unconventional reservoir examples, the Bell Creek Member of the Hare Indian Formation exhibits lower quartz and higher clay content, average bulk porosity, and lower N_2 pore volume. The results collectively suggest that high quartz and low clay content are the best predictors of porosity in the Horn River Group. Natural fractures may serve as flow pathways to induced fractures; however, these units lack the network of interconnected organic matter pores that can be present in other successions.

1. Introduction

Over the past two decades, the exploration of organic-rich mudstone intervals as unconventional hydrocarbon reservoirs has become increasingly prevalent. Owing to their apparent homogeneity at the core scale, several recently developed approaches are being used to investigate the properties of these units, including microfacies analysis at optical microscope- or scanning electron microscope (SEM)-scale (e.g., Egenhoff and Fishman, 2013; Biddle et al., 2021) and the use of geochemical proxies in chemostratigraphy (e.g., Ver Straeten et al., 2011; Ratcliffe et al., 2012; El Attar and Pranter, 2016; Turner et al., 2016; Playter et al., 2018; Harris et al., 2022). These techniques have revealed that fine-grained successions are in fact characterized by significant lateral and vertical variation. As with the methods employed in the study of coarser-grained intervals, the quantification of bulk porosity in prospective and producing organic-rich successions is important for modeling hydrocarbon storage capacity (Milliken and Curtis, 2016). In addition to the measurement of bulk porosity, the characterization of pore type, distribution, and origin through the use of SEM shows potential as a valuable tool for shedding further light on hydrocarbon storage (Ross and Bustin, 2009; Ambrose et al., 2010; Wang et al., 2013), permeability and flow pathways (Loucks et al., 2012; Han et al., 2016), wettability (Aplin and Macquaker, 2011; Begum et al., 2019), and wellbore stability (Curtis et al., 2012b), and is fundamental to the

* Corresponding author. Department of Earth and Atmospheric Sciences, University of Alberta, 1-26 Earth Sciences Building, Edmonton, Alberta, T6G 2E3, Canada.
E-mail address: maya1@ualberta.ca (M.T. LaGrange).

https://doi.org/10.1016/j.marpetgeo.2022.105738
Received 25 August 2021; Received in revised form 11 April 2022; Accepted 5 May 2022
Available online 13 May 2022

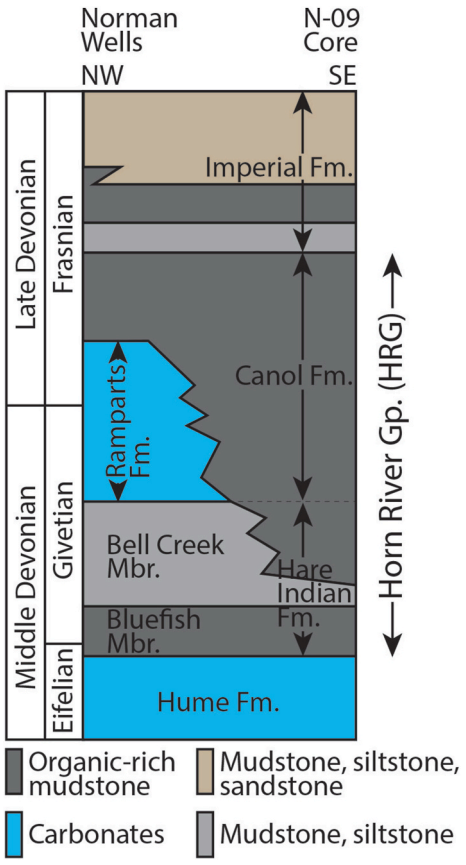

Fig. 1. Stratigraphic column of the Horn River Group in the Central Mackenzie Valley, Northwest Territories. Modified from Kabanov and Gouwy (2017) and Pyle and Gal (2016). Abbreviations: Fm. – Formation, Mbr. – Member, and Gp. – Group.
(For interpretation of the references to colour in this figure legend, the reader is referred to the Web version of this article.)

successful prediction of porosity in these units (Löhr et al., 2015; Milliken and Curtis, 2016).

In the central Northwest Territories (NWT) of Canada, the Middle to Late Devonian Horn River Group comprises the Hare Indian and Canol Formations, which are mudstones, and the Ramparts Formation, a carbonate interval (Fig. 1). With maximum thickness exceeding 300 m (e.g., Kabanov and Deblonde, 2019) and total organic carbon (TOC) values ranging from approximately 1 to 17 wt % (e.g., Pyle et al., 2015), this group comprises a world-class hydrocarbon resource roughly contemporaneous to many prolific mudstone reservoirs across North America. Although similarly named and age equivalent, the Horn River Group of the central NWT and Yukon comprises different formations than its southern counterpart, which is located approximately 600 km to the south in northeastern British Columbia (c.f. Dong et al., 2015). The Horn River Group of the NWT is also laterally equivalent to the prolific Middle to Late Devonian interval in Alberta, with the Canol Formation as the stratigraphic equivalent of the Duvernay Formation (Kabanov, 2019). In both the Horn River Group of British Columbia and the Duvernay Formation, porosity type and distribution have been described in detail (e.g., Dong et al., 2015; Dong et al., 2019; Knapp et al., 2020). In contrast, many questions remain about the nature of porosity in the Horn River Group of the central NWT. Particularly, the pore size, distribution, and degree of pore connectivity have not yet been assessed. Outstanding questions also surround the pore types and their origins as well as the controls and predictors of porosity in the Horn River Group. Finally, we do not yet understand how porosity in the Horn River Group compares to other North American unconventional mudstone reservoirs. To fill these gaps in knowledge, we investigate the porosity of organic-rich mudstone units in the Husky Little Bear N-09 core (N-09 core) from the Central Mackenzie Valley of the NWT (Fig. 2), which include the Hare Indian and Canol Formations of the Horn River Group, along with the basal Imperial Formation (Fig. 1). With respect to the Horn River Group interval in the N-09 core, the aims of this paper are fourfold: (1) porosity characterization and quantification, (2) interpretation of the origins of porosity, (3) identification of controls and predictors of porosity within the unit, and (4) comparison of porosity to other North American mudstone reservoirs. This study is the first detailed porosity characterization of Middle to Late Devonian mudstone strata in the frontier Northern Canadian Mainland Sedimentary Basin. Moreover, this work will ultimately facilitate the evaluation of reservoir potential in the Horn River Group of the NWT by allowing for more accurate hydrocarbon storage capacity estimates and contributing to our understanding of hydrocarbon flow pathways and wettability.

Many techniques used to measure porosity have limitations associated with the size range of resolvable pores (Milliken and Curtis, 2016; Katz and Arango, 2018). Nitrogen adsorption analysis is useful for studying mesopores (1–25 nm radius) and their distribution (Ross and Bustin, 2009; Mastalerz et al., 2013; Han et al., 2016), whereas He porosimetry resolves all pore sizes, including those smaller than 2 nm in diameter (micropores) (Mastalerz et al., 2013; Yang et al., 2016). The lowest pore diameter detected by SEM is approximately 5–15 nm (e.g., Keller et al., 2011; Klaver et al., 2015; Löhr et al., 2015; Han et al., 2016), which can exclude a significant proportion of the porosity in fine-grained assemblages (Keller et al., 2011; Milliken and Curtis, 2016; Katz and Arango, 2018). Nonetheless, direct imaging through SEM is useful for pore characterization (Milliken and Curtis, 2016) and can be used to support and verify results produced with indirect measurement techniques such as He and N_2 porosimetry (Schieber, 2013). Thus, we assess porosity using a combination of He porosimetry, N_2 adsorption experiments, and scanning electron microscopy (SEM).

This paper follows the nomenclature and mudstone naming scheme of Lazar et al. (2015), with 'mudstone' used as the generic name for fine-grained sedimentary rocks with >50% of grains smaller than 62.5 μm. Additionally, we use the pore type classification system of Loucks et al. (2012), which distinguishes three types of pores: (1) mineral matrix pores, which are subdivided into interparticle pores and intraparticle pores, (2) organic matter pores (intra-organic matter pores), (3) and fracture pores. The pore size distinctions put forth by the International Union of Pure and Applied Chemistry (e.g., Sing, 1982) are followed herein, classifying; (1) micropores (radius <1 nm), (2) mesopores (radius 1–25 nm), and (3) macropores (radius >25 nm).

2. Geological setting

The Middle to Late Devonian Horn River Group of the west-central NWT is a mixed mudstone-carbonate succession that includes the Hare Indian, Ramparts, and Canol Formations (Fig. 1; Pugh, 1983; Pyle and Gal, 2016; Kabanov and Gouwy, 2017). The Hare Indian Formation overlies the drowning unconformity at the top of the Hume Formation (Kabanov and Gouwy, 2017), and comprises the siliceous and organic-rich shales of the Bluefish Member, and the more argillaceous mudstones of the Bell Creek Member, both of which have variable carbonate content (Pyle and Gal, 2016). The overlying Ramparts Formation, a series of carbonate ramp, platform, and reef deposits (Muir et al., 1985), was deposited only in areas where the Hare Indian Formation is thickest and thus is locally absent in many cores in the Central Mackenzie Valley (Kabanov and Deblonde, 2019). The uppermost Horn River Group unit, the Canol Formation, is an organic-rich mudstone and the source of the conventional oil produced from the Norman Wells oil field, NWT, from the Kee Scarp Member of the Ramparts Formation (Snowdon et al., 1987). In the past two decades, interest has increased in the unconventional reservoir potential of the Canol Formation and the Bluefish Member of the underlying Hare Indian Formation. Preliminary

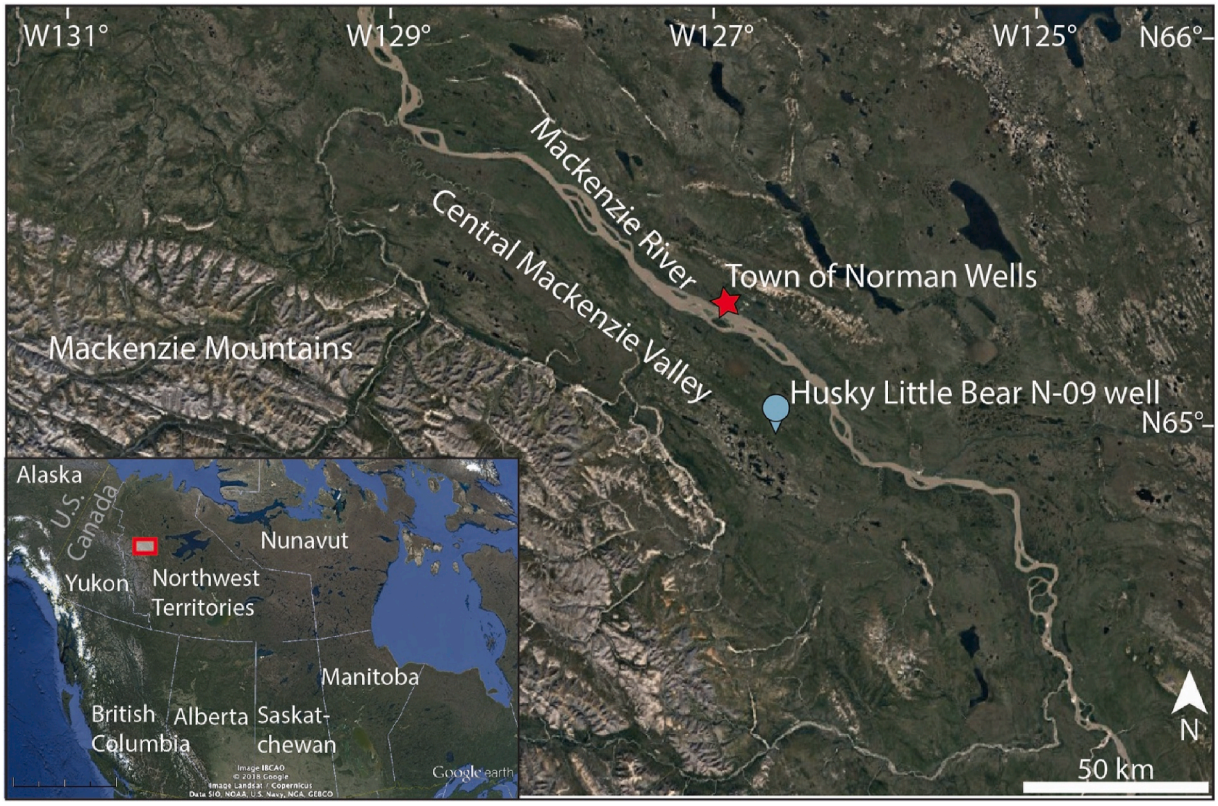

Fig. 2. Location map for the Husky Little Bear N-09 well in the Central Mackenzie Valley, Northwest Territories, Canada. Image modified from Google Earth Pro 7.1.8.3036 (2018). The study area is highlighted with a red box on the inset map and is shown in greater detail in the larger map. *Central Mackenzie Valley and Mackenzie Mountains, Northwest Territories, Canada.* 64°58′56.91" N, 127°49′26.08" W, Eye alt 323.9 km. Data SIO, NOAA, U.S. Navy, NGA, GEBCO. (Accessed October 4, 2019).
(For interpretation of the references to colour in this figure legend, the reader is referred to the Web version of this article.)

estimates by the National Energy Board and the Northwest Territories Geological Survey reported 145 and 46 billion barrels of oil in place for the Canol Formation and Bluefish Member, respectively (Northwest Territories Geological Survey and National Energy Board, 2015).

It is worth noting that this paper follows the stratigraphic nomenclature of Pyle and Gal (2016) for the Horn River Group. In the framework of Pyle and Gal (2016), the Hare Indian Formation comprises the lower Bluefish Member and upper Bell Creek Member, and the Canol Formation is not subdivided at the member level (Fig. 1). Kabanov and Gouwy (2017) produced a more detailed stratigraphic framework for the Horn River Group, with the upper Hare Indian Formation assigned to three different members, and two members distinguished in the Canol Formation, which is useful for stratigraphic correlation. Nonetheless, given that the present study is not stratigraphical in nature, these authors opt to use the simpler framework of Pyle and Gal (2016). Moreover, herein, the Bell Creek Member Dark Facies (Pyle and Gal, 2016), which is lithologically similar to the lower Canol Formation (Kabanov and Gouwy, 2017) and also termed the Prohibition Creek Member (Kabanov and Gouwy, 2017), is not distinguished from the Canol Formation.

This project focuses on the cored interval of the Horn River Group in the Husky Little Bear N-09 well, located at 64°58′55.2" N, 126°31′20.2" W in the Central Mackenzie Valley, NWT, Canada (Fig. 2), hereafter referred to as the N-09 core. In the Paleozoic, the present-day Central Mackenzie Valley was located along the northwestern margin of the Laurentian craton (Fraser and Hutchison, 2017). Following Neoproterozoic supercontinent breakup, a passive margin developed along the western and northern fringes of Laurentia, with the northern (Franklinian) margin transitioning to a convergent margin in the early Paleozoic (Hadlari et al., 2014a; Dewing et al., 2019). In the study area, early to middle Cambrian extension, which produced a graben system (MacLean, 2011), was followed by a period of subsidence and carbonate platform development from the late Cambrian to Middle Devonian (Fritz et al., 1991; MacLean et al., 2014). Devonian sediment accumulation in the study area occurred along the Mackenzie Platform (Fig., 3; Lenz, 1972; Norris, 1985), which was separated from the Porcupine Platform to the west by the Richardson Trough (Fig., 3; Lenz, 1972; Jeletzky, 1975; Pugh, 1983).

Leading up to the Middle Devonian, shallow-water carbonate deposition occurred on the Mackenzie Platform, while organic-rich mudstones and carbonates accumulated in the Richardson Trough (Pugh, 1983). Deposition of the Horn River Group was initiated in the latest Eifelian with drowning of the Hume Formation carbonates, which were succeeded by the organic-rich mudstone of the Bluefish Member (Kabanov and Gouwy, 2017; Morrow, 2018). In areas where the Hare Indian Formation mudbank was thickest, deposition of the Ramparts Formation carbonates began (Kabanov, 2019; Fig. 1) and continued with the onset of another marine transgression (Muir et al., 1985; Morrow, 2018). Meanwhile, the organic-rich Canol Formation was deposited in off-bank areas (Kabanov and Gouwy, 2017). Ultimately, this transgression led to drowning of the Ramparts carbonates and onlapping of the Canol Formation (Muir and Dixon, 1984; Muir et al., 1985; Yose et al., 2001). Horn River Group deposition concluded in the Late Devonian as the Ellesmerian Orogeny along the northern margin of Laurentia transformed the study area into a foreland basin and initiated deposition of the siliciclastic Imperial Formation, which overlies this group (Garzione et al., 1997; Beranek et al., 2010).

Peak thermal conditions during burial of the Horn River Group are interpreted to have taken place prior to the Cretaceous (Issler et al., 2005; Powell et al., 2020). Subsequent cooling and uplift produced a

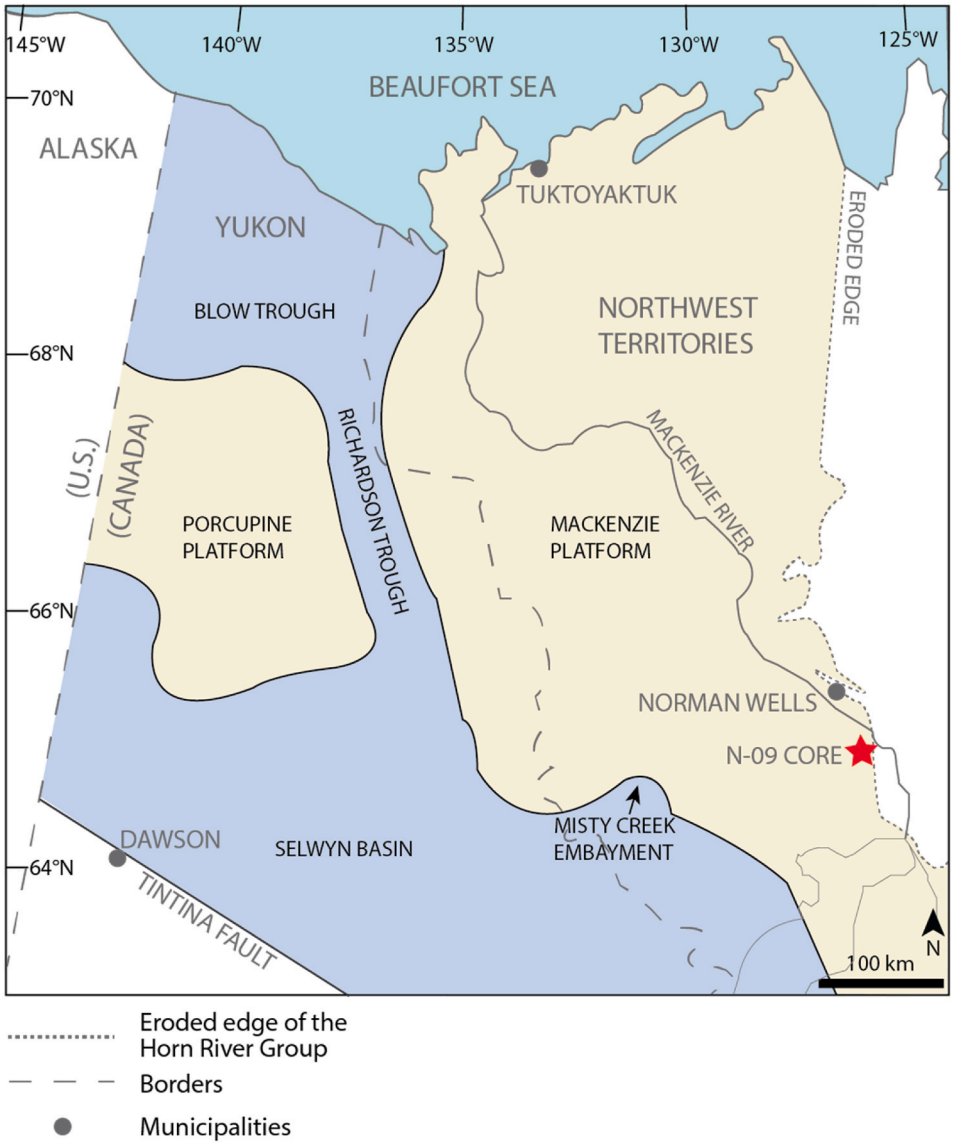

Fig. 3. Structural features of the study area during the Middle to Late Devonian. Black lines and text represent modern-day geography, whereas grey lines and text indicate paleogeographic features during the Middle to Late Devonian. After Pugh (1983), Al-Aasm et al. (1996), and Morrow (2018).
(For interpretation of the references to colour in this figure legend, the reader is referred to the Web version of this article.)

Table 1
Samples characterized through N_2 porosimetry and SEM imaging from the N-09 core.

Depth (m)	Name	Lithofacies	Formation	Group
1670.28	F3A	3	Imperial	N/A (overlies Horn River Group)
1687.00	F5A	5	Imperial	N/A (overlies Horn River Group)
1708.20	F5B	5	Canol	Horn River
1715.25	F1A	1	Canol	Horn River
1727.05	F2A	2	Canol	Horn River
1751.00	F3B	3	Canol	Horn River
1799.35	F1B	1	Canol	Horn River
1810.00	F4A	4	Hare Indian (Bell Creek Member)	Horn River
1820.40	F4B	4	Hare Indian (Bell Creek Member)	Horn River
1825.00	F2B	2	Hare Indian (Bluefish Member)	Horn River

regional sub-Cretaceous unconformity, which was again followed by burial and erosion associated with the North American Cordillera foreland basin (Powell et al., 2020) produced by orogenesis in the Jurassic and Cretaceous (Hadlari et al., 2014b). Beginning in the Miocene, accretion of the Yakutat terrane to the North American craton in the Gulf of Alaska area caused ongoing crustal shortening in the study area (Mazzotti and Hyndman, 2002).

3. Data and methods

The slabbed, vertical core retrieved from the N-09 well is 167.8 m in length and includes the upper few metres of the Hume Formation, the entire Horn River Group (Hare Indian and Canol and Formations), and the lowermost Imperial Formation. Analytical methods consisted of sedimentological descriptions and the collection of samples to assess mineralogy, thermal maturity, and porosity.

3.1. Composition analysis

X-ray diffraction (XRD) analysis on 59 core samples was performed

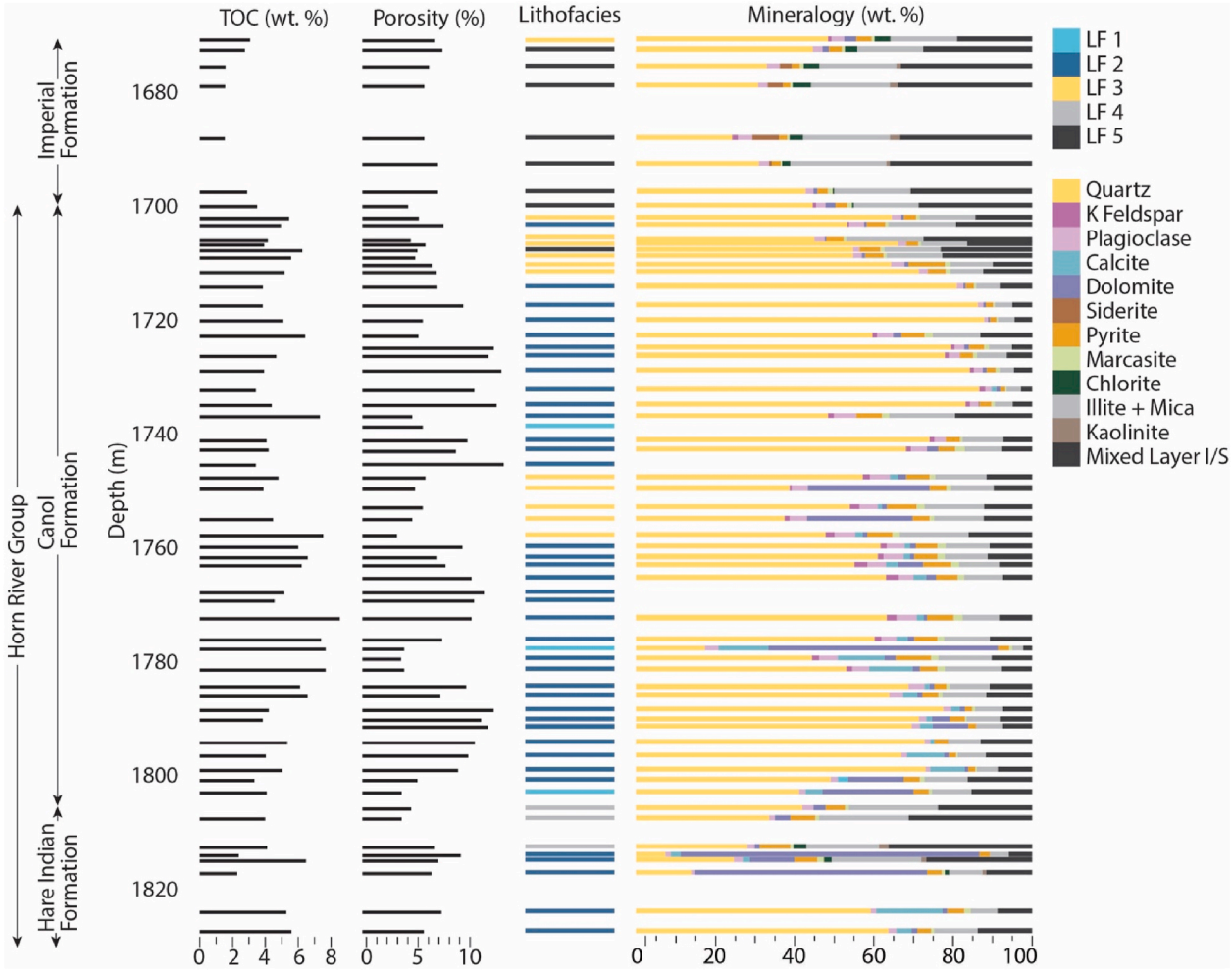

Fig. 4. TOC, porosity, mineralogy, and lithofacies with depth in the N-09 core. Porosity values are bulk porosity measurements using the Gas Research Institute (GRI) method. Acronyms: LF– lithofacies, mixed layer I/S–mixed-layer illite-smectite, and TOC–total organic carbon.
(For interpretation of the references to colour in this figure legend, the reader is referred to the Web version of this article.)

by Core Laboratories Canada. Samples were analyzed using a Philips automated powder diffractometer. Semi-quantitative determination of mineral abundance was performed using integrated peak areas and empirical reference intensity ratio factors. TOC measurements were collected for 55 samples with a LECO analyzer by Core Laboratories Canada. See Appendix A for extended methods.

3.2. Lithofacies

Detailed sedimentological observations of the N-09 core focused on lithology, bedding and laminae, fissility, fossils and trace fossils, and diagenetic features such as nodules. Core colour was described following the 2009 Munsell Geological Rock-Color Chart (Rock-Color Chart Committee, 2009). These observations were then synthesized to define lithofacies following the scheme outlined in Lazar et al. (2015), which names fine-grained sedimentary rocks according to grain size and then applies modifiers to describe bedding, composition, and other attributes (e.g., colour). To characterize the dominant composition of each lithofacies, the relative proportions of quartz, total clay, and carbonate (calcite and dolomite) were determined for each of the 59 samples analyzed by x-ray diffraction.

3.3. Thermal maturity

Vitrinite Reflectance (VRo) data for six samples were collected by Core Laboratories Canada using a Zeiss Axio Imager A2M microscope equipped with a CRAIC CoalPro Microspectrophotometer. Samples were first pulverized to 850 μm and then mixed with epoxy resin and hardener. Following hardening, these samples were ground and polished with a Buehler AutoMet 250 instrument. Measurements from certain samples used vitrinite, whereas others were made on graptolite and converted following Bertrand (1990) or on bitumen and converted using the Jacob Formula (VRo = BRo x 0.618 + 0.4) where BRo is bitumen reflectance in oil. Several particles were measured for each sample and the reported VRo is the mean value. Please see the extended methods (Appendix A) for further detail.

Source rock evaluation parameters (S1, S2, S3, and T_{max}) were measured by Core Laboratories Canada with a Rock-Eval 6 instrument. Sample preparation was the same as described for TOC measurements. Hydrogen Index (HI) was calculated using S2 and TOC values and Oxygen Index (OI) was calculated using S3 and TOC values (e.g., Tissot and Welte, 1984; Law et al., 1999).

3.4. Scanning electron microscope imaging

Samples from ten depths (Table 1) were investigated using SEM, comprising two representative samples from each of the five lithofacies. The selected samples are displayed in Table 1 along with lithofacies and lithostratigraphic information. Samples are named with their lithofacies number and either 'A' or 'B' (Table 1). Because of the fissile nature of

Table 2
Summary of the sedimentological, paleontological, and ichnological characteristics of each observed lithofacies.

Description	Sedimentology and Accessories	Fossils and Bioturbation
F1: Medium grey planar parallel-laminated siliceous calcareous to calcareous mudstone	• Planar parallel laminae, more commonly continuous but sometimes discontinuous • Non-fissile	• No fossils observed • Bioturbation not observed at this scale
F2: Brownish black continuous planar parallel-laminated siliceous mudstone with common calcareous laminae and centimetre-scale carbonate beds	• Planar parallel laminae common, most often continuous • May also appear homogeneous • Common calcareous/dolomitic laminae or cm-scale limestone/dolostone beds • Common calcite/dolomite and pyrite nodules (often have both carbonate and pyrite in the same nodule) • Pyrite streaks sometimes present • Low–moderate fissility	• Rarely, pyritized Tentaculitids are observed on bedding planes • Bioturbation not observed at this scale
F3: Brownish black continuous planar parallel-laminated siliceous mudstone	• Continuous planar parallel laminae are common but sometimes also appears homogeneous • Pyrite nodules common • Rare limestone/dolostone nodules • Abundant pyrite streaks • Low–moderate fissility	• No fossils observed • Bioturbation not observed at this scale
F4: Medium dark grey homogeneous-appearing fissile argillaceous mudstone	• Homogenous appearing • Occasional calcareous and dolomitic laminae or cm-scale beds • Occasional pyrite nodules • Moderate–high fissility	• None observed • Bioturbation not observed at this scale
F5: Medium grey homogeneous appearing highly fissile argillaceous mudstone with common fossil fragments	• Often appears homogeneous but planar parallel laminae also present in some intervals • Pyrite nodules common • High fissility	• Organic fragments and fossil fragments (including *Spathiocaris*) common on bedding planes • Bioturbation not observed at this scale

Lithofacies 5, the sample from depth 1708.2 m (F5B), was analyzed parallel to bedding, whereas all other samples were analyzed perpendicular to bedding. Core pieces were polished through Broad Ion Beam (BIB) milling using Ar ions with a Fischione Model 1060 SEM Mill. Backscattered electron (BSE), secondary electron (SE), and InLens imagery of the carbon-coated core pieces were obtained using a Zeiss Sigma 300 VP scanning electron microscope with an accelerating voltage of 15 kV and an aperture of 30 μm. Energy-dispersive X-ray spectroscopy (EDS) with a Bruker XFlash 6160 was used to characterize the elemental composition of components assessed using SEM.

3.5. Porosimetry

Bulk porosity was measured by Core Laboratories Canada for 64 samples following the Gas Research Institute (GRI) methodology (e.g., Luffel and Guidry, 1993). Additionally, ten core samples comprising two of each lithofacies were selected for low-pressure N_2 adsorption measurements (Table 1). Equivalent surface areas were determined using the Brunauer–Emmett–Teller (BET) method (Brunauer et al., 1938) and pore size distributions were calculated following Density Functional Theory (DFT; e.g., Olivier et al., 1994). See Appendix A for extended methods.

3.6. Multivariate statistical analysis

For this study, multivariate statistics were used to assess the covariance between several properties of the Horn River Group in the N-09 core including porosity, mineralogy, lithofacies, and TOC. Highly skewed variables were first log-transformed. The PCAmixdata package of R (https://cran.r-project.org/web/packages/PCAmixdata/PCAmixdata.pdf) was then used to perform analysis on a mixture of quantitative and categorical data, which involves a combination of two different methods: Principal Component Analysis (PCA) and Multiple Correspondence analysis (MCA; Chavent et al., 2015). PCA extracts the most important information from a data table composed of quantitative inter-related variables and from this produces principal components (dimensions), which comprise statistically independent linear combinations of the variables. From this, the relationships between different variables can be displayed (Abdi and Williams, 2010). In contrast, MCA allows for the analysis of relationships between categorical variables (Abdi and Valenti, 2007). PCAmix provides a means to illustrate covariance in a multivariate dataset comprised of both quantitative and qualitative properties (Chavent et al., 2015).

4. Results

Fig. 4 gives the TOC, porosity, lithofacies, and mineralogy with depth in the N-09 core for each depth that a GRI bulk porosity measurement was taken. These results are also presented in Appendix B (Table B1).

4.1. Lithofacies

Five lithofacies are identified in the N-09 core. The characteristics of each lithofacies are summarized in Table 2 and illustrated in Fig. 5. Fig. 4 displays the lithofacies observed at each depth associated with a GRI porosity reading. In Appendix B Table B1, the normalized total clay, carbonate, and quartz of each XRD sample are shown along with the corresponding compositional classification following Lazar et al. (2015), which was used to guide the lithofacies compositional names.

4.2. Composition

Fig. 4 and Table B1 (Appendix B) show mineralogy and TOC with depth in the N-09 core, with TOC values ranging from 1.54 wt % to 8.63 wt %. For the purposes of this discussion, we use low (0–30%), moderate (30–60%), and high (60–100%) to describe mineral abundance. The mineralogical dataset shows that the Horn River Group in the N-09 core is composed primarily of siliceous mudstone, with certain intervals dominated by argillaceous or calcareous mudstone (Fig. 4). Lithofacies 1 has moderate to high carbonate content (Fig. 6). Most samples from

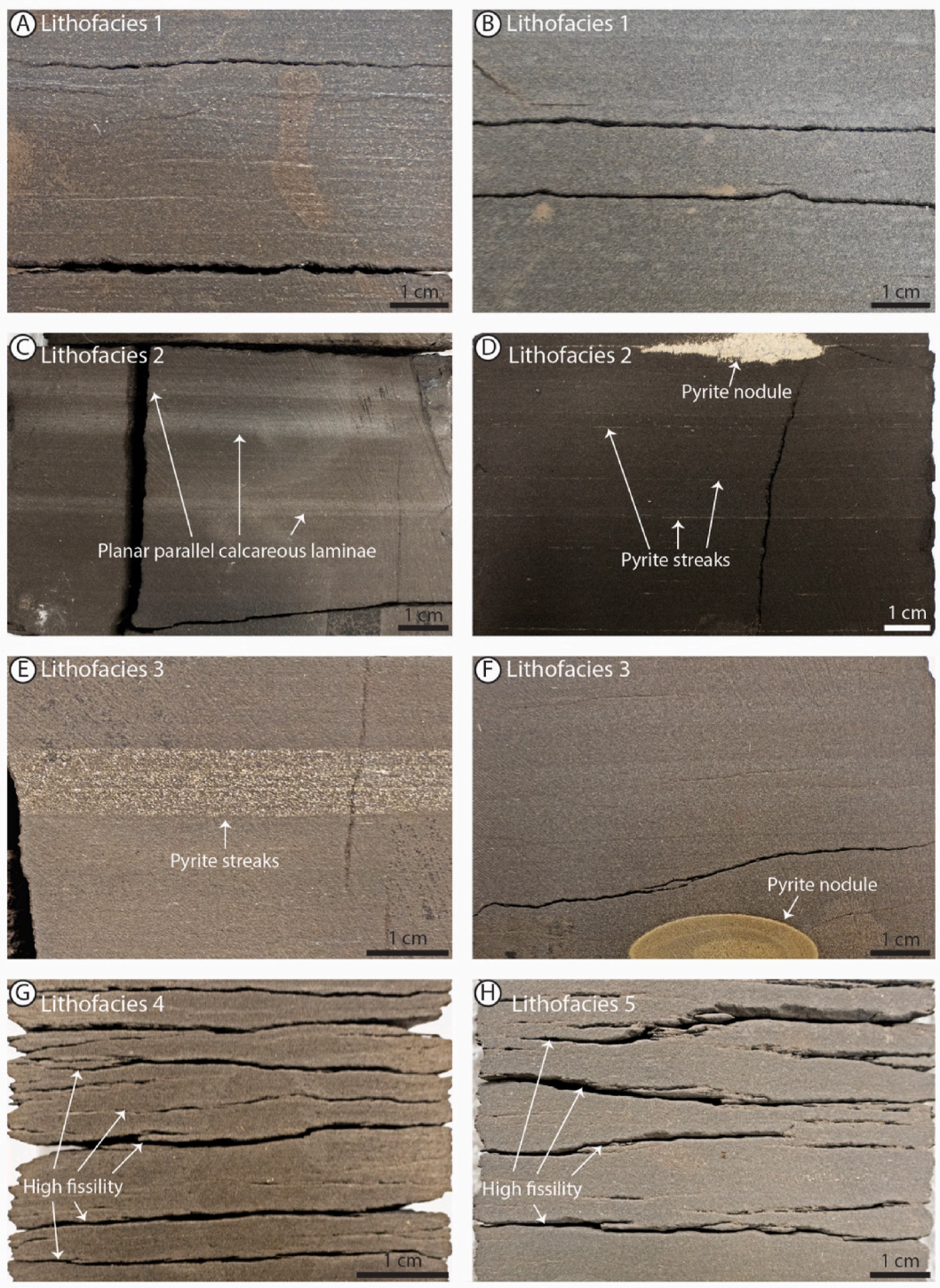

Fig. 5. Representative core photographs illustrating the five different lithofacies present in the N-09 core. (A) Lithofacies 1 at 1777.3 m, (B) Lithofacies 1 at 1709.45 m, (C) Lithofacies 2 at 1765.4 m, (D) Lithofacies 2 at 1745.5 m, (E) Lithofacies 3 at 1704.45 m, (F) Lithofacies 3 at 1753.05 m, (G) Lithofacies 4 at 1810.15 m, (H) Lithofacies 5 at 1696.3 m.
(For interpretation of the references to colour in this figure legend, the reader is referred to the Web version of this article.)

Lithofacies 2 have high quartz and low carbonate content, although a few are characterized by a high proportion of carbonate, likely because of the common calcareous/dolomitic laminae and centimetre-scale beds associated with this lithofacies (Fig. 6). Lithofacies 3 is siliceous with low carbonate and a moderate to low abundance of clay, whereas Lithofacies 4 and 5 are argillaceous with moderate quartz content (Fig. 6).

4.3. Thermal maturity

Source rock evaluation parameters are displayed in Table 3. On a pseudo-Van Krevelen diagram (Fig. 7), these samples plot near the origin of the graph, typically indicating maturity (Law, 1999) and making it difficult to interpret the original kerogen type. Nonetheless, petrographic analyses of Bluefish Member and Canol Formation samples from 16 locations in the Central Mackenzie Valley by Snowdon et al.

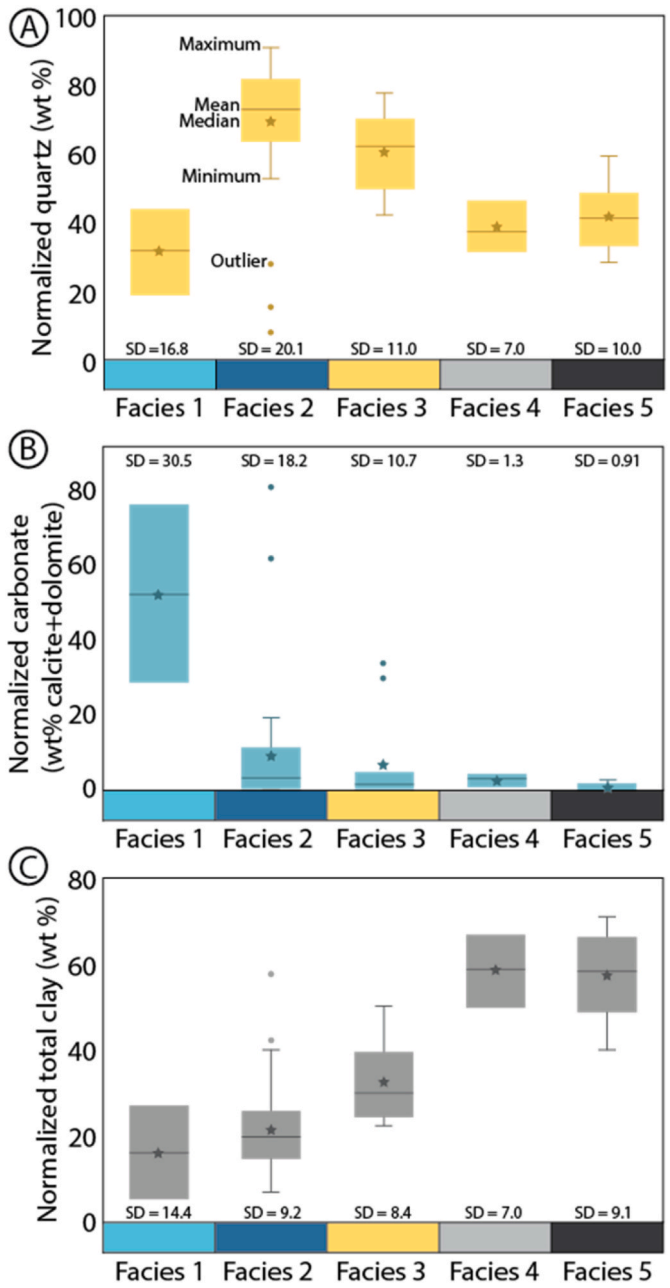

Fig. 6. Mineralogy per lithofacies. Quartz, clay, and carbonate (calcite + dolomite) were normalized to 100%. The upper bar represents the maximum, the lower bar is the minimum, the horizontal line denotes the median, and the star highlights the mean. Outliers are shown with points. Acronyms: SD−standard deviation.
(For interpretation of the references to colour in this figure legend, the reader is referred to the Web version of this article.)

(1987) showed that organic matter in both those units is primarily Type II. Herein, vitrinite reflectance values range from 1.02 to 1.29% R_o (Table A1), which places these samples in the late oil window (Tissot and Welte, 1984; Dembicki, 2009). The T_{max} values show an overall increasing trend with depth and range from 458 to 472 °C (Table 3), characteristic of the late oil window to early gas window (Espitalié et al., 1985).

Table 3
Source rock evaluation and TOC results. Acronyms: HI–Hydrogen Index, OI–Oxygen Index, TOC–Total Organic Carbon. HI is calculated as follows: S2 x 100/TOC. OI is calculated as follows: S3 x 100/TOC.

Depth (m)	Leco TOC (wt. %)	Rock-Eval S1 (mg HC/g)	Rock-Eval S2 (mg HC/g)	Rock-Eval S3 (mg CO2/g)	Tmax (°C)	HI	OI
1,692.58	2.22	0.53	1.54	0.17	458	69	8
1,710.08	7.94	0.19	3.32	0.10	464	42	1
1,724.50	4.31	0.27	1.63	0.06	461	38	1
1,738.45	2.24	0.14	0.81	0.19	470	36	8
1,752.53	6.94	0.88	3.80	0.12	466	55	2
1,765.07	5.95	0.16	3.07	0.10	466	52	2
1,779.04	8.89	0.26	4.55	0.12	468	51	1
1,791.31	3.38	0.13	1.07	0.13	467	32	4
1,805.38	6.17	0.47	4.02	0.08	472	65	1
1,820.00	4.55	0.82	2.81	0.13	472	62	3

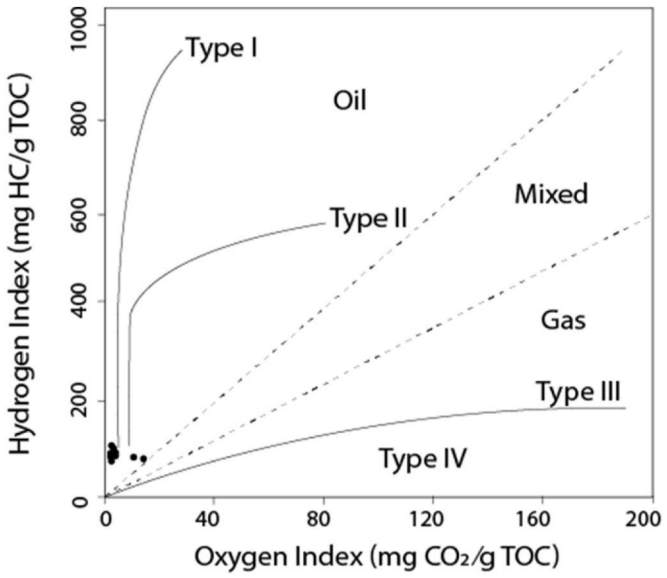

Fig. 7. A pseudo-Van Krevelen diagram for the Horn River Group in the N-09 core. Fields on the plot (kerogen type trends and dashed lines denoting oil, mixed, and gas zones) are following Dembicki (2009).
Acronyms: HC–Hydrocarbon, TOC–Total Organic Carbon.

4.4. GRI porosity

Porosity readings for the 64 samples analyzed with the GRI method are displayed in Fig. 4 and in Table B1 (Appendix B). The porosity of the Horn River Group and lower Imperial Formation in the N-09 core ranges from 3.2% to 13.1%. Mean porosity is highest in Lithofacies 2, although this lithofacies displays a wide range of porosities (Fig. 8 A). The lowest mean porosity is observed in Lithofacies 1 (Fig. 8A). In the Canol Formation, mean porosity is 7.7%, with the highest standard deviation of the lithostratigraphic units considered (Fig. 8 B). The Bell Creek Member of the Hare Indian Formation displays a mean porosity of 5.2%, whereas the Bluefish Member of this same formation has an average porosity of 7.1% (Fig. 8 B).

4.5. Pore types observed with scanning electron microscopy

The following section uses the pore type classification of Loucks et al. (2012), which classifies pores as (1) mineral matrix pores, subdivided into interparticle pores and intraparticle pores, (2) organic matter pores (intra-organic matter pores), (3) and fracture pores. For all samples, the mineral matrix comprises mainly quartz and clay minerals (Fig. 9 A–I),

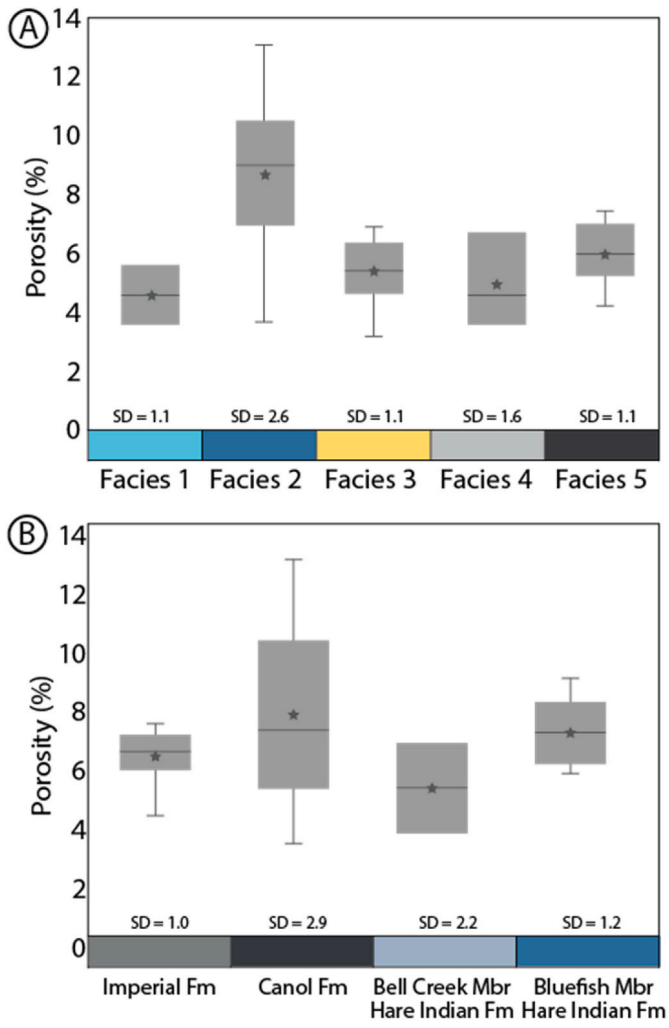

Fig. 8. Gas Research Institute (GRI) method bulk porosity per (A) lithofacies and (B) lithostratigraphic unit in the N-09 core. The upper bar represents the maximum, the lower bar is the minimum, the horizontal line denotes the median, and the star highlights the mean. Outliers are shown with points. Acronyms: SD – standard deviation.
(For interpretation of the references to colour in this figure legend, the reader is referred to the Web version of this article.)

aside from sample F1B, which contains a high proportion of dolomite (Fig. 9 J). In varying proportions, pyrite, carbonates (primarily dolomite), and calcareous or pyritized microfossils (e.g., Tentaculitids in sample F4B; Fig. 9 D) are also present in the observed samples (Fig. 9). At SEM scale, the sedimentary fabric in both samples from Lithofacies 2 (F2A and F2B) and sample F3A consists of planar laminae defined by pyrite (Fig. 9 E, G, H). No clear fabric is observed at SEM scale in the Lithofacies 1 samples (F1A and F1B), the second Lithofacies 3 sample (F3B), the Lithofacies 4 samples (F4A, and F4B), or either Lithofacies 5 sample (F5A, F5B).

Loucks and Reed (2014) presented several criteria to distinguish migrated organic matter from original depositional organic matter. Criteria associated with migrated organic matter (solid bitumen or pyrobitumen) include (1) organic matter present where cementation has already occurred, (2) organic matter filling intraparticle pores, (3) spongy texture, (4) abundant connected organic matter-filled pores, (5) pores within organic matter that are not aligned, (6) devolatilization cracks in organic matter, and (7) anomalously large bubbles, which are formed when oil or gas is trapped in migrated organic matter (Loucks and Reed, 2014). All samples of the Horn River Group in this study appear to contain migrated organic matter. This interpretation stems from the presence of organic matter within pores that contain authigenic mineral growth (criterion 1, Fig. 10 A and B), organic matter infilling intraparticle pores (criterion 2, Fig. 10 C), pores within organic matter that are irregularly distributed and lack alignment (criterion 5, Fig. 10 D, E, and F) and the common presence of crack-like pores in organic matter (criterion 6, Fig. 10 E–H).

In addition to organic matter pores (Fig. 10), SEM analysis also revealed the presence of mineral matrix pores (interparticle and intraparticle) in the observed samples (Figs. 11 and 12). Many interparticle pores are partially filled by authigenic minerals such as pyrite, clay, or dolomite and migrated organic matter (e.g., Fig. 11). Intraparticle pores are observed within clay platelets (e.g., Fig. 12 A and B), dolomite crystals (e.g., Fig. 12 C), pyritized microfossil fragments (e.g., Fig. 12 D), and in pyrite framboids (e.g., Fig. 12 E and F). Pyritized microfossil fragments may comprise hyalosponge spicules, which have been observed in the Horn River Group (Kabanov and Jiang, 2020), tentaculitids, which are common in the Bluefish Member of the Hare Indian Formation (Muir and Dixon, 1984; Pyle and Gal, 2016), or Ovummuridea, which are documented in Late Devonian strata of the southern Northwest Territories (MacNeil and Jones, 2006). In two dimensions, the observed interparticle, intraparticle, and organic matter pores are either irregular in shape or crack/slit-like (Figs. 10–12). In SEM view, these pores are isolated and do not show connectivity to one another (Figs. 10–12).

Fractures pores at the SEM-scale are present in samples F5A, F4B, and F3B (Fig. 9 A, D, and F respectively) and EDS showed that they are filled only with epoxy and do not contain mineral cement. Additionally, open fractures are observed on a larger scale (centimetres to decimeters in length) at several depths throughout the N-09 core. Fractures are present in Lithofacies 1, 2, and 3, but are not observed in Lithofacies 4 and 5 (Fig. 13). Some of these fractures show connectivity in core, but others are isolated (Fig. 13). From previous outcrop and core observations, the Horn River Group of the study area is known to be naturally fractured, with both open and cemented fractures present (e.g., Irish and Kempthorne, 1987; Yose et al., 2001; Hadlari et al., 2015). These fractures were produced by exhumation from the compressional tectonic regime associated with the ongoing collision of the Yakutat terrane and the North American Plate (Hadlari et al., 2015). Thus, although it is possible that some of the fractures observed herein may be drilling-induced (or in the case of the SEM samples, caused by sample preparation), many of them are likely naturally occurring.

4.6. N_2 adsorption analysis

Fig. 14 shows the mesopore volume of all ten samples analyzed with N_2 adsorption-desorption experiments. Both samples from Lithofacies 1 (F1A and F1B) show intermediate pore volume relative to the other samples. Pore volume from Lithofacies 2 is variable, with sample F2A plotting amongst the highest pore volume results and samples F2B showing one of the lowest pore volumes. Similarly, sample F3A from Lithofacies 3 has the highest pore volume, whereas the other Lithofacies 3 sample (F3B) shows low pore volume. Samples from Lithofacies 5 (F5A and F5B) plot near one another, exhibiting low total pore volume and the same pattern is observed for samples from Lithofacies 4 (F4A and F4B). Mesopore size distribution results are presented in Fig. 15. The highest mesopore volume is hosted by pores around 2 nm in all samples except for F4A and F2A, which both show slightly higher peaks near 2.5 nm.

Adsorption hysteresis describes a deviation of the adsorption isotherm from the desorption isotherm (Sing, 1982). The N_2 adsorption and desorption isotherms for all samples analyzed are displayed in Fig. 16. All isotherms show a similar shape to International Union of Pure and Applied Chemistry hysteresis loop type H3 (Appendix A Fig. A1), suggesting that the pores in these samples are slit-shaped. Many pores observed with SEM are also slit-shaped (e.g., Fig. 10 A, B, G, and H, some pores in Fig. 10 A and B, some pores in Fig. 11 C and D, and some

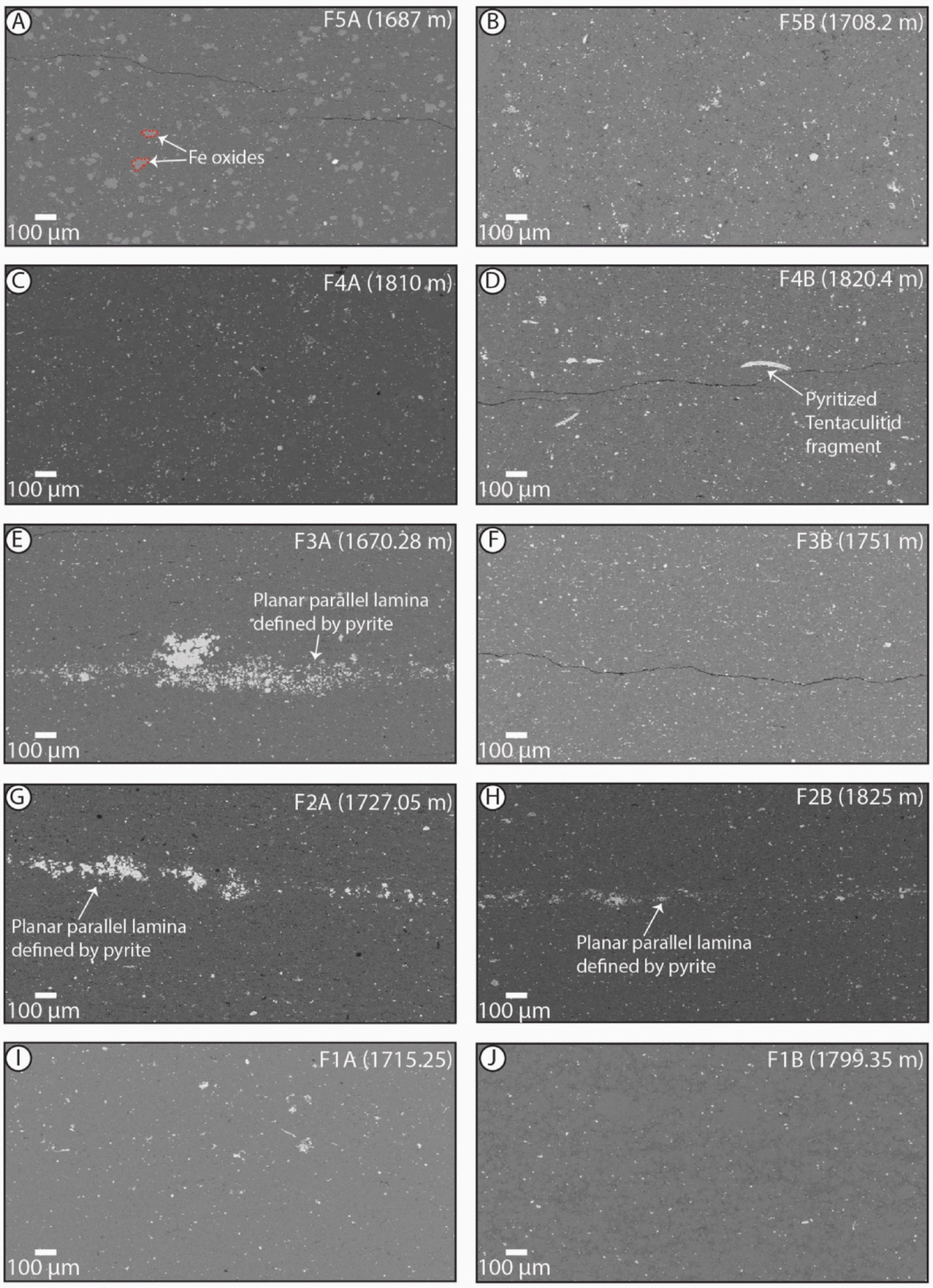

Fig. 9. Overview of the sedimentary fabrics observed in ten samples from the N-09 core through scanning electron microscope (SEM) imaging. All images are captured with the backscattered-electron detector.

pores in Fig. 12 A and B) although others are irregular (e.g., Figs. 10 E and Fig. 11 A and B, some pores in Fig. 11 C and D, Fig. 12 C, D, E, and F and some pores in Fig. 12 A and B). This difference in shape between pores observed with SEM compared to the interpreted pore shape from hysteresis loops is likely attributed to a difference in scale. Most of the pores observed with SEM are macropores and range from tens of nanometers to several micrometres in radius (e.g., Figs. 10, Fig. 11, Fig. 12), whereas the N_2 adsorption technique characterized mesopores (1–25 nm), with the highest mesopore volume at approximately 2 nm.

4.7. PCAmix

Fig. 17 displays the relationships between qualitative variables (lithofacies) and quantitative variables (porosity, TOC, and mineralogy) from the Horn River Group of the N-09 core. Dimensions represent directions along which the dataset varies most (James et al., 2013). Herein, dimension 1 explains 23.27% of the variance in the dataset, dimension 2 accounts for 20.45%, and dimension 3 explains 12.79%. Fig. 17 A shows that porosity appears to be correlated most closely with

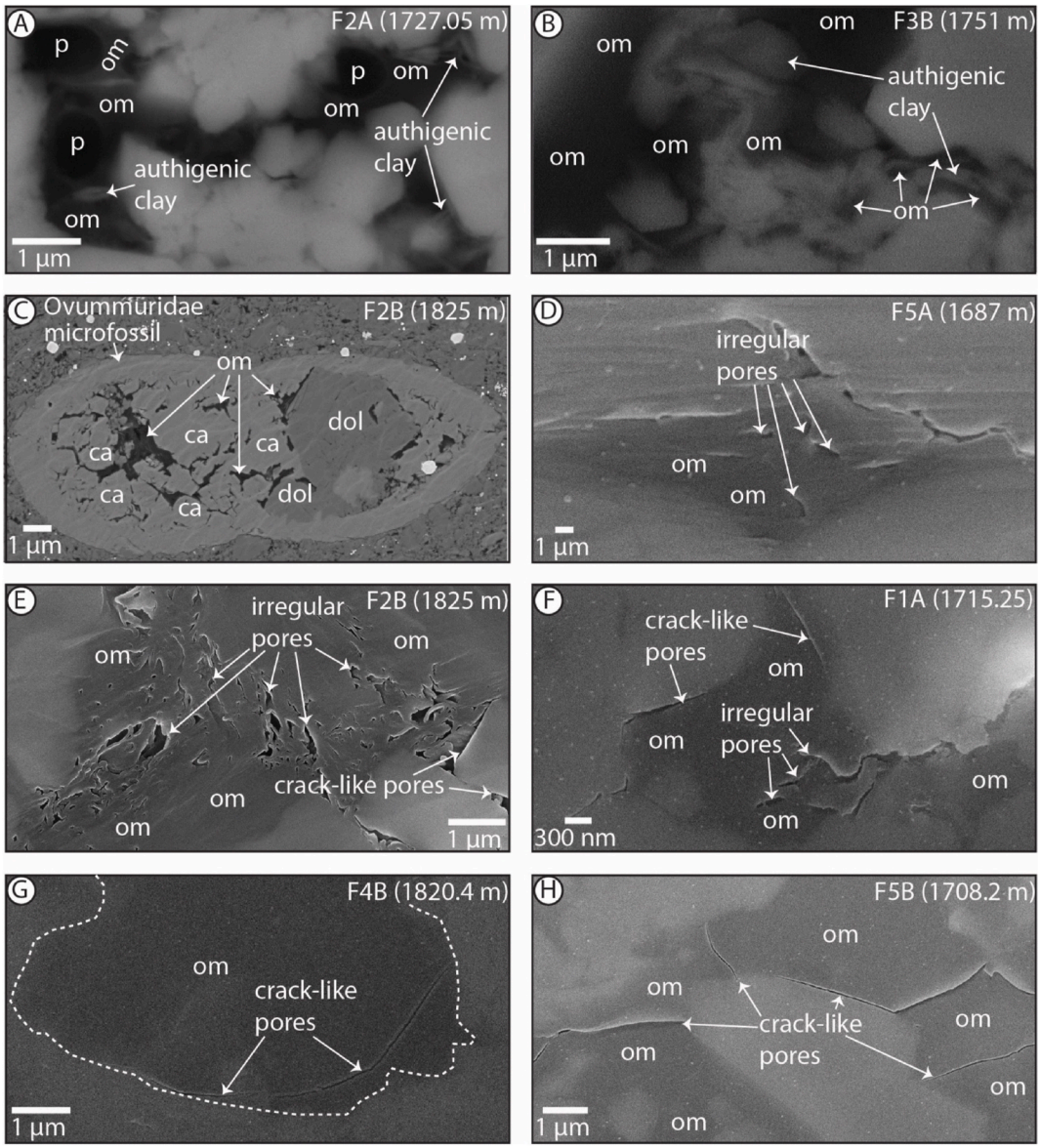

Fig. 10. Organic matter in the observed samples from the N-09 core captured with a scanning electron microscope (SEM). (A) and (B) show organic matter in interparticle pores along with authigenic clay minerals. (C) displays organic matter filling intraparticle pores within a microfossil (possibly Ovummuridae). (E) displays irregular organic matter pores while (E) and (F) display primarily irregular organic matter pores with a few crack-like pores. Crack-like organic matter pores are shown in (G) and (H). Images (A)–(C) were captured with the backscattered electron detector, whereas images (F)–(H) used the InLens detector. Abbreviations: ca – calcite, dol – dolomite, om – organic matter, and p – pore.

the abundance of quartz and total clay. Similarly, Fig. 17 B shows that porosity is closely related to the abundance of quartz. Further discussion of the relationships between variables shown in Fig. 17 is beyond the scope of this study.

5. Discussion

5.1. Porosity origins

In the Horn River Group, and particularly the Canol Formation, biogenic silica is often prevalent (Pyle and Gal, 2016) in the form of recrystallized radiolarian tests (e.g., MacKenzie, 1974; Kabanov, 2019; Biddle et al., 2021). Mudstone intervals rich in biogenic silica can undergo reduced compaction compared to more clay-rich units because of increased cementation and/or higher rigidity (Schieber, 2013; Dong et al., 2015, 2017; Milliken and Curtis, 2016; Liu et al., 2020; Knapp et al., 2020). Enhanced rigidity associated with abundant biogenic silica is a likely explanation for the prevalence of interparticle pores observed with SEM.

Pyrite framboids are a host of intraparticle porosity in the samples examined for this study (Fig. 12 E and F). Pyrite framboids can form either in the euxinic water column (syngenetic pyrite) or in sediment during diagenesis (Wignall and Newton, 1998; Suits and Wilkin, 1998; Roychoudhury et al., 2003). Previous interpretations of paleoredox conditions during deposition of the Horn River Group mudstone units suggested persistent euxinia, citing as evidence sedimentological attributes such as horizontal, apparently unbioturbated beds and laminae, and the prevalence of disseminated euhedral and framboidal pyrite (e.g., Tassonyi, 1969; Al-Aasm et al., 1996); and geochemical evidence such as high TOC and high degree of pyritization values (Al-Aasm et al., 1996), high % S to % TOC ratios (Snowdon et al., 1987), and trace metal enrichment (e.g., Mo and U; Kabanov and Gouwy, 2017; Kabanov, 2019). These studies did not examine sedimentological or ichnological characteristics at the thin section scale. However, Biddle et al. (2021)

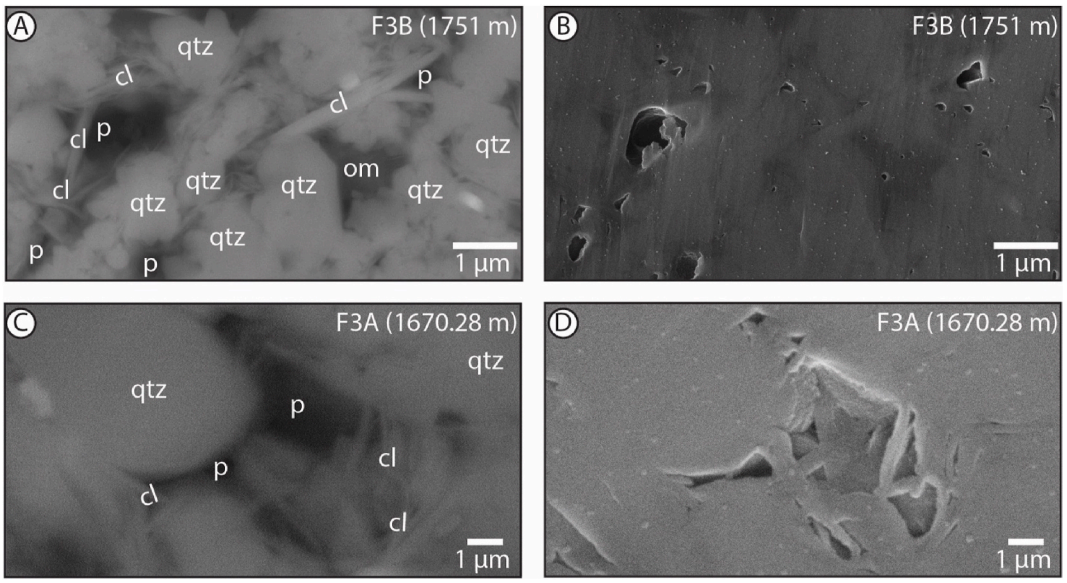

Fig. 11. Interparticle pores observed in the N-09 core through scanning electron microscope (SEM) imaging. The top two images show interparticle pores containing authigenic clay minerals and organic matter from sample F3B with (A) the back-scattered electron detector and (B) the InLens detector. The bottom images are interparticle pores from Sample F3A with (C) the back-scattered electron detector and (D) the InLens detector. Abbreviations: cl – clay, om – organic matter, p – pore, and qtz – quartz.

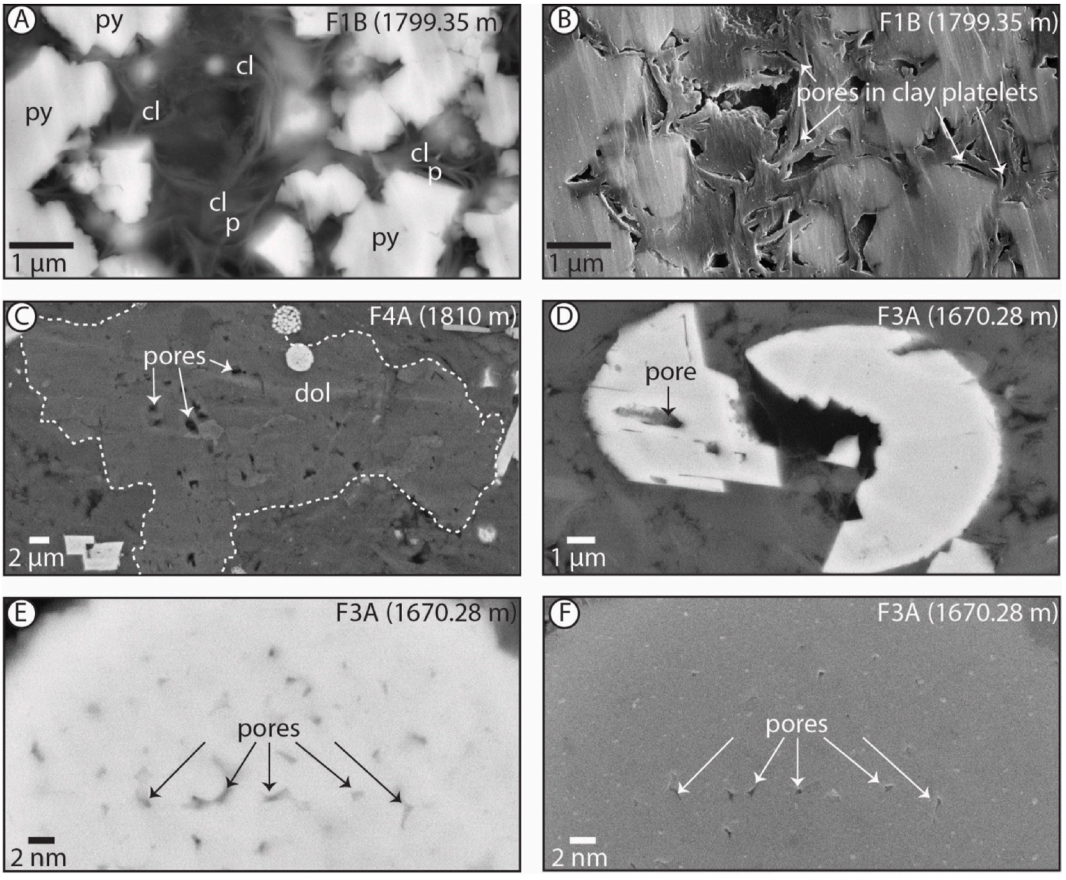

Fig. 12. Scanning electron microscope (SEM) images of intraparticle pores in the studied samples. (A) shows intraparticle pores in clay platelets with the back-scattered electron detector and (B) is from the sample depth using the InLens detector. Intraparticle pores are also displayed in (C) a dolomite crystal (outlined with a white dashed line), (D) a microfossil, and (E) a pyrite framboid. The same area as shown in (E) with the back-scattered electron detector is displayed in (F) with the InLens detector. Abbreviations: cl – clay, dol – dolomite, and p – pore.

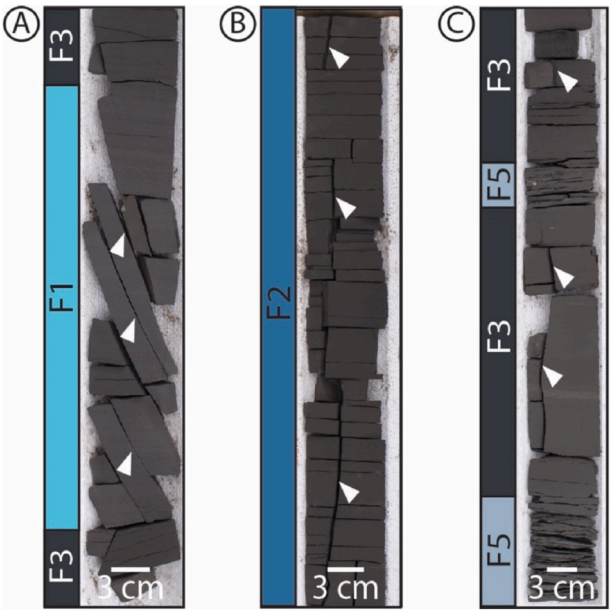

Fig. 13. Macroscale fractures (white triangles) in the N-09 core (A) 1754.86 m–1755.29 m, (B) 1763.59 m–1765.47 m, (C) 1704.04–1704.65 m. Definitions: F1 – Lithofacies 1, F2 – Lithofacies 2, F3 – Lithofacies 3, F5 – Lithofacies 5. (For interpretation of the references to colour in this figure legend, the reader is referred to the Web version of this article.)

presented an ichnological study of thin sections taken from several Horn River Group drill cores in the Central Mackenzie Valley, including the N-09 core discussed herein and observed the presence of micro-bioturbation in many of the mudstone intervals. They concluded that at the time of deposition, dissolved oxygen levels in bottom waters likely ranged from 0.0 to 0.1 ml/l, corresponding to severe dysoxia to anoxia. Although other proxies suggest persistent euxinic conditions, this indicates that euxinia was likely intermittent at most with seasonal increases in sea floor oxygenation potentially associated with storms (Biddle et al., 2021). Similarly, based on the presence of benthic hyalosponge spicules in the Horn River Group, Kabanov and Jiang (2020) interpreted that the anoxic and/or euxinic conditions (suggested by geochemical and sedimentological proxies) were interrupted by periods of weak seafloor oxygenation. Thus, some of these pyrite framboids may have formed in the water column, whereas others originated in the sediment during diagenesis. The rigid nature of pyrite likely resulted in the preservation of intraparticle porosity within these framboids, despite compaction.

Intraparticle pores in this interval are also commonly observed in calcite and dolomite, with a noticeably higher abundance in samples F1B and F4A (e.g., Fig. 12 C). Organic acids, such as carboxylic acids, produced during thermal maturation of buried biomass, are a likely cause for the partial dissolution of carbonate grains (MacGowan and Surdam, 1990; Schieber et al., 2016; Li et al., 2018a). Clay platelets also host intraparticle pores in these samples, particularly in the authigenic clay minerals infilling interparticle porosity (e.g., Fig. 12 A and B), which are likely a result of smectite to illite transformations.

Organic matter pores can be primary in origin (present in original depositional kerogen) or secondary, which are produced later from thermal cracking (Milliken et al., 2013; Löhr et al., 2015; Katz and Arango, 2018). Primary organic matter porosity is believed to depend on kerogen maceral type (Curtis et al., 2012a), and it has been suggested that secondary organic matter porosity develops in response to thermal cracking of depositional kerogen or secondary thermal cracking of migrated organic matter (Canter et al., 2016). The observed organic matter pores in the N-09 core are more likely to have been produced by thermal cracking because the host organic matter has characteristics suggestive of migration rather than original depositional kerogen. Crack-like pores found in organic matter or at the organic matter-mineral interface have been interpreted to form as devolatilization fractures during oil generation (e.g., Sondergeld et al., 2013), although several authors have also suggested that these crack-like pores are an artifact produced through desiccation or devolatilization during core retrieval and sample preparation (e.g., Fishman et al., 2012; Loucks et al., 2012; Loucks and Reed, 2014) or ion-milling (e.g., Schieber, 2013; Klaver et al., 2016).

Subvertical natural fractures are abundant in the Horn River Group of the Central Mackenzie Valley, with a primary orientation trending to the NE–SW and secondary NW–SE trend (Fig., 18; Irish and Kempthorne, 1987; Hadlari, 2015). In the N-09 core, these fractures are lithofacies-dependant (Fig. 13) and are more prevalent in the Canol Formation than in the underlying Hare Indian Formation. Natural fractures are thought to have formed during exhumation associated with thrust faulting that developed in response to the ongoing collision of the Yakutat terrane with the North American Plate, beginning in the Miocene (Hadlari, 2015).

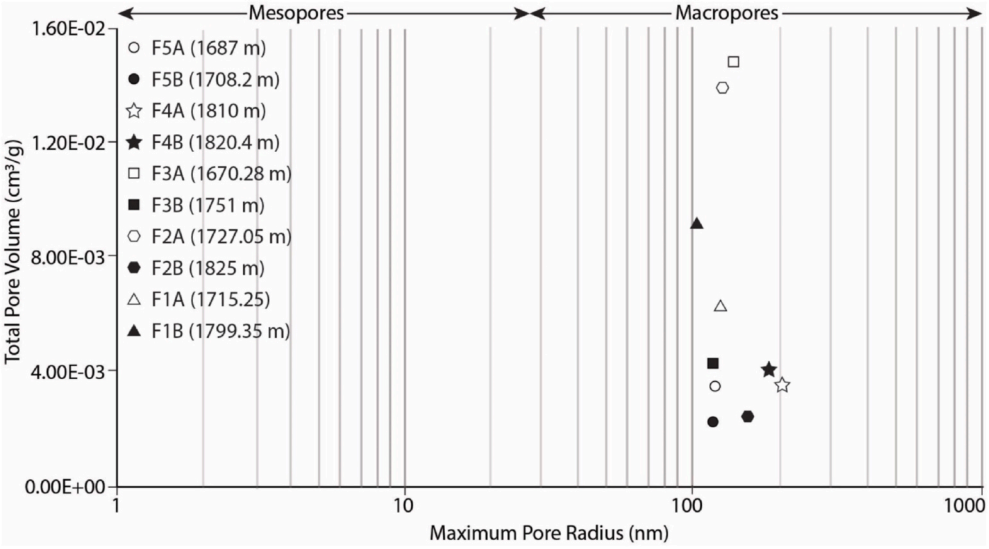

Fig. 14. Mesopore volume results from N_2 adsorption and desorption experiments. Total pore volume includes pores smaller than the indicated maximum pore radius.

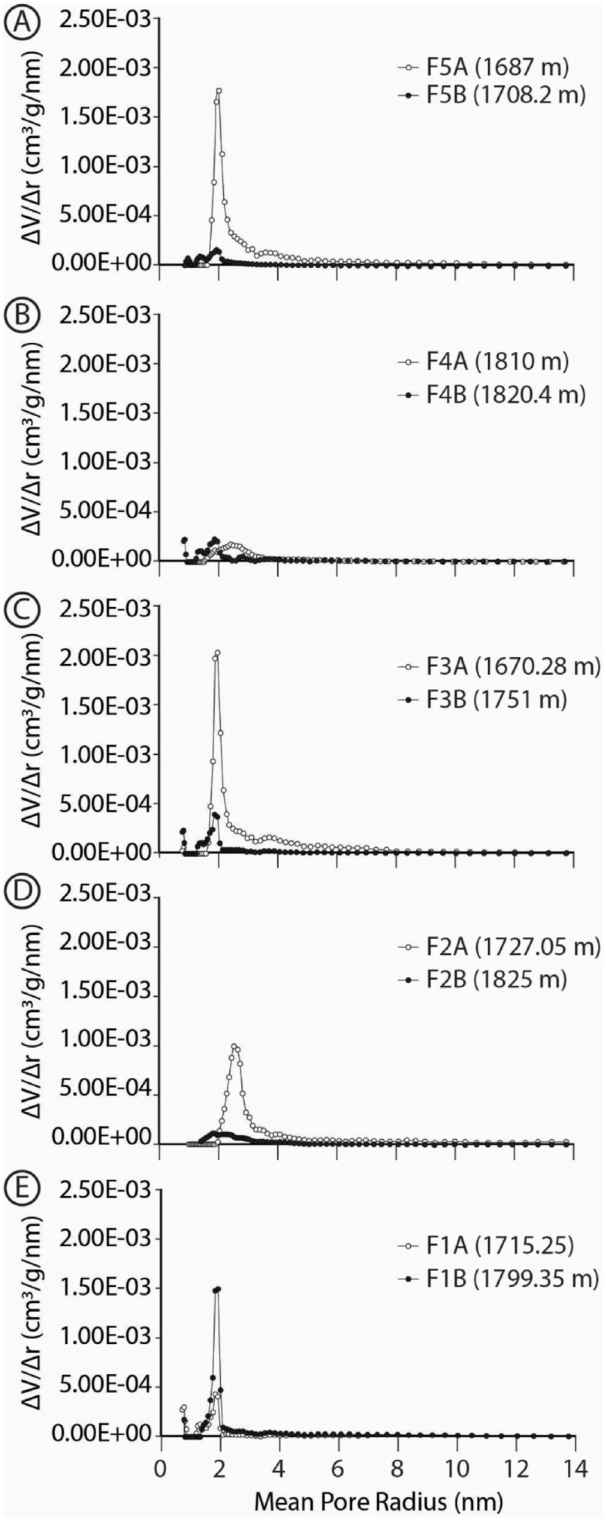

Fig. 15. Mesopore size distribution by volume determined from N_2 adsorption and desorption experiments using Density Functional Theory (DFT; e.g., Olivier et al., 1994). Definitions: V – total pore volume, r – mean pore radius.

In sum, the abundance and type of pores in the Horn River Group evolved as the sediment underwent compaction, burial diagenesis, and subsequent structural deformation. First, terrigenous sediment was deposited along with varying proportions of radiolarian tests, siliceous hyalosponge spicules, carbonate microfossils (e.g., tentaculitids), organic matter, and possibly pyrite framboids that formed in the water column during intermittent periods of euxinia. Early diagenesis of organic-rich mud commonly produces framboidal pyrite and carbonate precipitation (non-ferroan calcite and dolomite) through anaerobic microbial respiration (Konhauser, 2007; Macquaker et al., 2014). The products of these reactions are observed in the Horn River Group, particularly framboidal pyrite and dolomite (e.g., Biddle et al., 2021). Compaction would have reduced interparticle porosity, with smaller pores more likely to be preserved than larger pores (Yang and Aplin, 2007; Emmanuel and Day-Stirrat, 2012). Starting at burial temperatures of approximately 20–60 °C, biogenic opal-A transforms to Opal-CT and then eventually to quartz (Keller and Isaacs, 1985; Williams and Crerar, 1985). Abundant biogenic silica in this interval, particularly in the Canol Formation and Bluefish Member of the Hare Indian Formation (Pyle and Gal, 2016; Harris et al., 2022), may have reduced the degree of pore compaction through enhanced rigidity (Aplin and Macquaker, 2011; Schieber, 2013; Dong et al., 2015, 2017; Milliken and Curtis, 2016; Knapp et al., 2020). The rigidity of pyrite framboids also appears to have preserved some intraparticle porosity in these grains. During burial diagenesis, smectite to illite transformations occur between approximately 50–100 °C, producing authigenic clay cement (Hower et al., 1976; Hover et al., 1996), and forming the intraparticle pores within authigenic clay platelets observed herein. Organic acids produced during catagenesis would have resulted in some degree of carbonate dissolution at burial temperatures of about 80–120 °C (MacGowan and Surdam, 1990; Schieber et al., 2016; Li et al., 2018a), forming intraparticle pores, like those in Fig. 12 C. Final developments in porosity would have included the development of devolatilization cracks in organic matter from oil migration, natural fracture development induced by terrane accretion beginning in the Miocene (Hadlari, 2015), and possibly desiccation cracks in organic matter following core retrieval.

5.2. Controls and predictors of porosity

Cross plots of porosity with quartz content, carbonate content, and total clay content suggest that of these factors, quartz content has the highest correlation with porosity, with an r^2 value of 0.3 (Fig. 18 A, C, and E). However, the relatively low r^2 values (0.3) observed for quartz–porosity suggests that other factors complicate this relationship. If samples with carbonate content exceeding 20 wt % and total clay content exceeding 30 wt % are excluded, the correlation coefficient between quartz and porosity increases and it is clear that clay and carbonate also influence porosity (Fig. 18 B). Negative covariation between clay and porosity is apparent for samples with clay content below 30 wt % (r^2 of 0.5, excluding carbonate-rich samples; Fig. 18 F). Whereas for samples containing greater than 30 wt % total clay, no obvious trend is present and all samples with total clay above 30 wt %. are characterized by porosity between ~ 4 and 8% (Fig. 18 F). A threshold may be present at approximately ~30 wt % clay abundance, above which the degree of compaction was higher because of greater ductility associated with the clay minerals. Plots of illite and mica versus porosity and mixed layer illite/smectite versus porosity show similar patterns with a negative trend observed only in samples with a lower abundance of these clay minerals (Fig. 18 G and H). The carbonate–porosity cross plots display a low r^2 value (Fig. 18 C and D) likely reflecting a complex relationship between carbonate content and porosity, with the dissolution of carbonates by organic acids generating secondary intraparticle pores, but diagenetic precipitation of carbonates filling porosity. These interpretations are also supported by the PCAMix results, which show quartz and total clay plotting near porosity, indicating a higher correlation compared to dimensions that plot further away (Fig. 17).

Many previous studies of organic-rich mudstone units have also found that silica is a primary control on porosity. For example, Dong et al. (2015) interpreted that the positive correlation between silica and porosity in the Horn River Group of British Columbia arises either from covariance between TOC and biogenic silica, or from the presence of

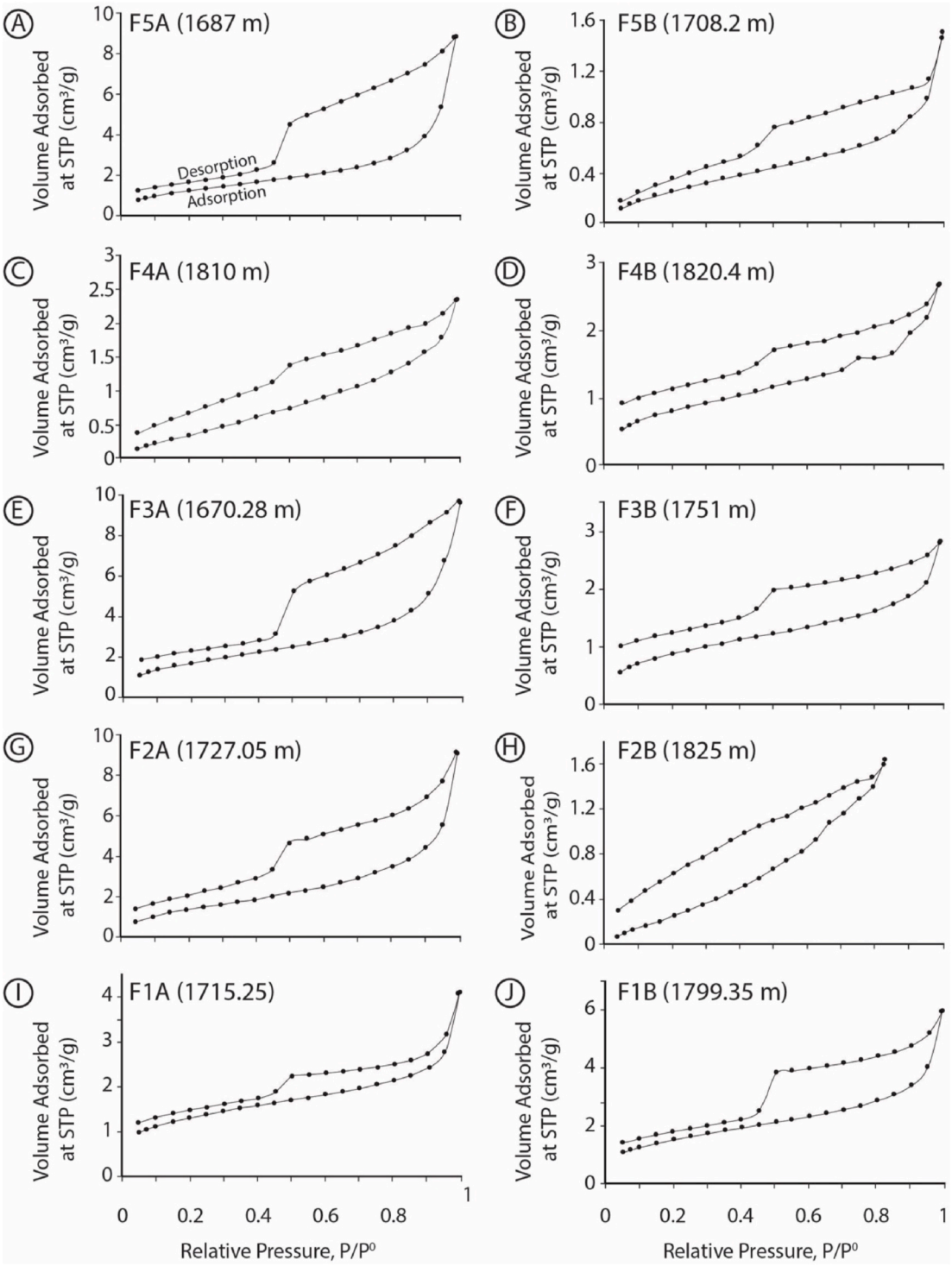

Fig. 16. The relationship between the volume of N_2 adsorbed/desorbed and the N_2 equilibrium pressure for ten Horn River Group samples. Acronyms and definitions: STP – standard temperature and pressure, p^o – saturation pressure of N_2 at 77 K.

silica cement preventing the collapse of intraparticle pores between clay platelets. Similarly, Li et al. (2018b) explained differences in porosity and pore distribution between lithofacies by suggesting that although most matrix mineral pores (interparticle and intraparticle between clay platelets) collapse during compaction, interparticle pores between authigenic silica grains are more resistant to this process, leading to higher porosity in authigenic silica-rich lithofacies and lower porosity in units with a higher proportion of clay. Moreover, the findings of some authors have led them to suggest that higher silica content also leads to increased preservation of organic matter pores through greater resistance to mechanical compaction (e.g., Wang et al., 2013; Fishman et al., 2012). Specifically, Knapp et al. (2020) found that biogenic silica is associated with higher organic porosity and greater pore size in the Duvernay Formation and interpreted this to be the product of reduced compaction. Thus, the silica present in the Horn River Group likely influenced porosity by leading to greater preservation of both matrix mineral porosity and organic porosity during mechanical compaction. Conversely, the observed negative covariation between clay mineral

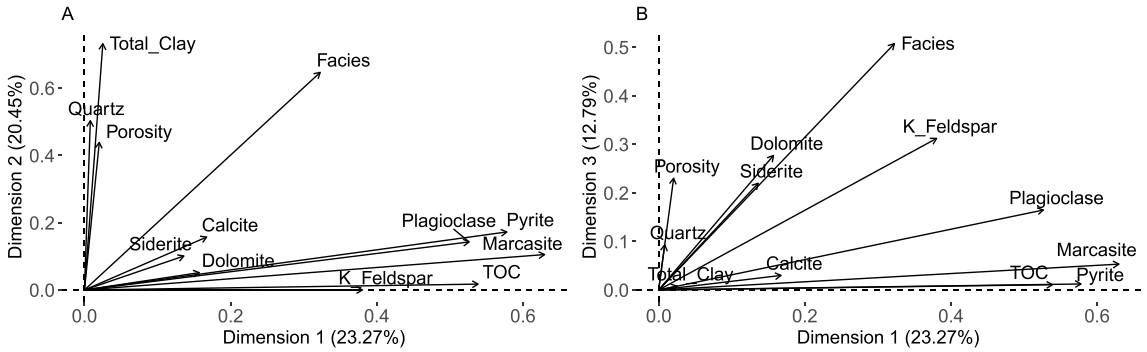

Fig. 17. Results from multivariate statistical analysis (PCAmix) showing the covariance between porosity, mineralogy, TOC, and lithofacies (labelled 'facies') in relation to (A) dimension 1 and dimension 2, and (B) dimension 1 and dimension 3. Porosity values are bulk porosity measurements calculated with the Gas Research Institute (GRI) method.

abundance and bulk porosity likely arises because of increased ductility and mineral matrix pore collapse in clay-rich intervals.

Unlike many other organic-rich mudstone resources worldwide, TOC is not a significant predictor of bulk porosity in the Horn River Group of the N-09 core ($r^2 = 0.02$ in Fig. 19 A; Fig. 17). For example, a relationship between TOC and bulk porosity is observed in the Marcellus Formation of Pennsylvania (e.g., Milliken et al., 2013), the Horn River Group of British Columbia (e.g., Dong et al., 2015), and the lower Cambrian to upper Ordovician strata of the Sichuan Basin, China (e.g., Wang et al., 2013; Yang et al., 2016; Li et al., 2018b). In all the above examples, organic matter pores comprised a dominant fraction of all pores (Milliken et al., 2013; Wang et al., 2013; Dong et al., 2015; Yang et al., 2016). Thus, a lack of TOC – bulk porosity relationship in the samples herein is suggestive of a lower relative abundance of organic matter pores in the N-09 core of the Horn River Group compared to the studied sections of the Marcellus Formation, the Horn River Group of British Columbia, and lower Cambrian to upper Ordovician strata of the Sichuan Basin.

There are a few possible explanations for a comparatively lower abundance of organic matter pores. First, a limited relative abundance of organic matter pores compared to other pore types was also observed in the Kimmeridge Clay Formation of the North Sea by Fishman et al. (2012), who suggested that a higher relative abundance of ductile components (e.g., kerogen and clay) compared to rigid components (e.g., silica or feldspar) may explain a lack of preservation of organic matter pores produced during hydrocarbon generation. Taking this a step further, Löhr et al. (2015) proposed that organic matter concentrated in laterally continuous laminae is more prone to loss of organic matter porosity due to greater ductile deformation. In the case of the Horn River Group in the N-09 core, the possibility of high plasticity resulting in greater destruction of organic matter pores compared to other organic-rich intervals does not seem likely. The quartz content associated with the Horn River Group in the N-09 core is comparable to or higher than that of other such intervals for both the Bluefish Member and the Canol Formation (Fig. 20). Moreover, a significant proportion of this silica is thought to be biogenic in origin for both the Bluefish Member and the Canol Formation (e.g., Pyle and Gal, 2016; Kabanov and Gouwy, 2017), which is believed to enhance the preservation of organic porosity (Knapp et al., 2020). For these reasons, mineralogy and sedimentary fabric are not plausible explanations for a low abundance of organic matter pores and lack of TOC–porosity correlation.

A second potential reason for a low proportion of organic matter pores in the Horn River Group of the N-09 core could be the nature of the original organic matter associated with these samples. It has been proposed that the potential for development of organic porosity varies based on kerogen type (e.g., Curtis et al., 2012a; Loucks et al., 2012; Chen et al., 2015; Klaver et al., 2016; Li et al., 2018b) and previous work suggests that organic matter pores are more common in type II kerogen than type III kerogen (Loucks et al., 2012; Lu et al., 2015). Nonetheless, organic matter in this interval is interpreted as primarily type II (Snowdon et al., 1987). Hence, it is unlikely that the type of organic matter present in the Horn River Group of the N-09 core is responsible for the comparatively lower proportion of organic matter pores relative to other mudstone reservoirs.

Thirdly, Löhr et al. (2015) observed a lower relative abundance of organic matter pores in the oil-mature samples of the Woodford Formation of Oklahoma compared to those in the gas window. Upon further investigation, this is likely explained by the infilling of organic matter pores with migrated bitumen in oil-mature samples, making these pores difficult to discern with SEM imaging, and subsequent expulsion of this bitumen as thermal maturity increases (Löhr et al., 2015). The N-09 core is within the geographic area interpreted as the oil window by Hadlari et al. (2015). Moreover, Rock-Eval Pyrolysis and vitrinite reflectance results from this study suggest that the N-09 core is in the late-oil to early-gas window, and thus, it is possible that bitumen has infilled organic pores and is masking their presence.

Thermal maturity has also been suggested as a controlling factor for organic porosity (e.g., Loucks et al., 2009; Curtis et al., 2012a; Mastalerz et al., 2013; Schieber, 2013; Klaver et al., 2016), although a clear relationship between thermal maturity and organic porosity has not typically been observed in organic-rich mudstone successions (see Katz and Arango, 2018 for an in-depth review of previous work surrounding thermal maturity and organic porosity). Nonetheless, in this case, there does appear to be some small degree of negative covariation between porosity and vitrinite reflectance (a proxy for thermal maturity), with an r^2 value of 0.1 (Fig. 19 B). Seeing as there is typically a linear relationship between depth and vitrinite reflectance (Carr, 2000; Dembicki, 2009), it is unusual that vitrinite reflectance shows some degree of correlation with porosity (Fig. 19 B), whereas the relationship between depth and porosity is significantly weaker (Fig. 19 C). This discrepancy may arise from changing levels of dissolved oxygen in bottom waters as the Horn River Group was deposited. Paleoredox conditions manifest control on vitrinite reflectance because dissolved oxygen availability affects the nature of early diagenetic biodegradation of vitrinite precursors (Fermont, 1988; Carr, 2000). The observed weak correlation between vitrinite reflectance and porosity may stem from the association of redox conditions and mineralogy, which are both at least in part related to the environmental conditions during deposition.

Related to both mineralogy and organic matter character or abundance is the influence of lithofacies on porosity. Recently, relationships between lithofacies and bulk porosity have been confirmed in certain fine-grained organic-rich successions, including the Horn River Group of British Columbia, Canada (Dong et al., 2015) and the Wufeng and Longmaxi Formations of South China (Li et al., 2018b). For the Horn River Group of the N-09 core, there appears to be a relationship between lithofacies and porosity (Fig. 17), with the highest porosity samples

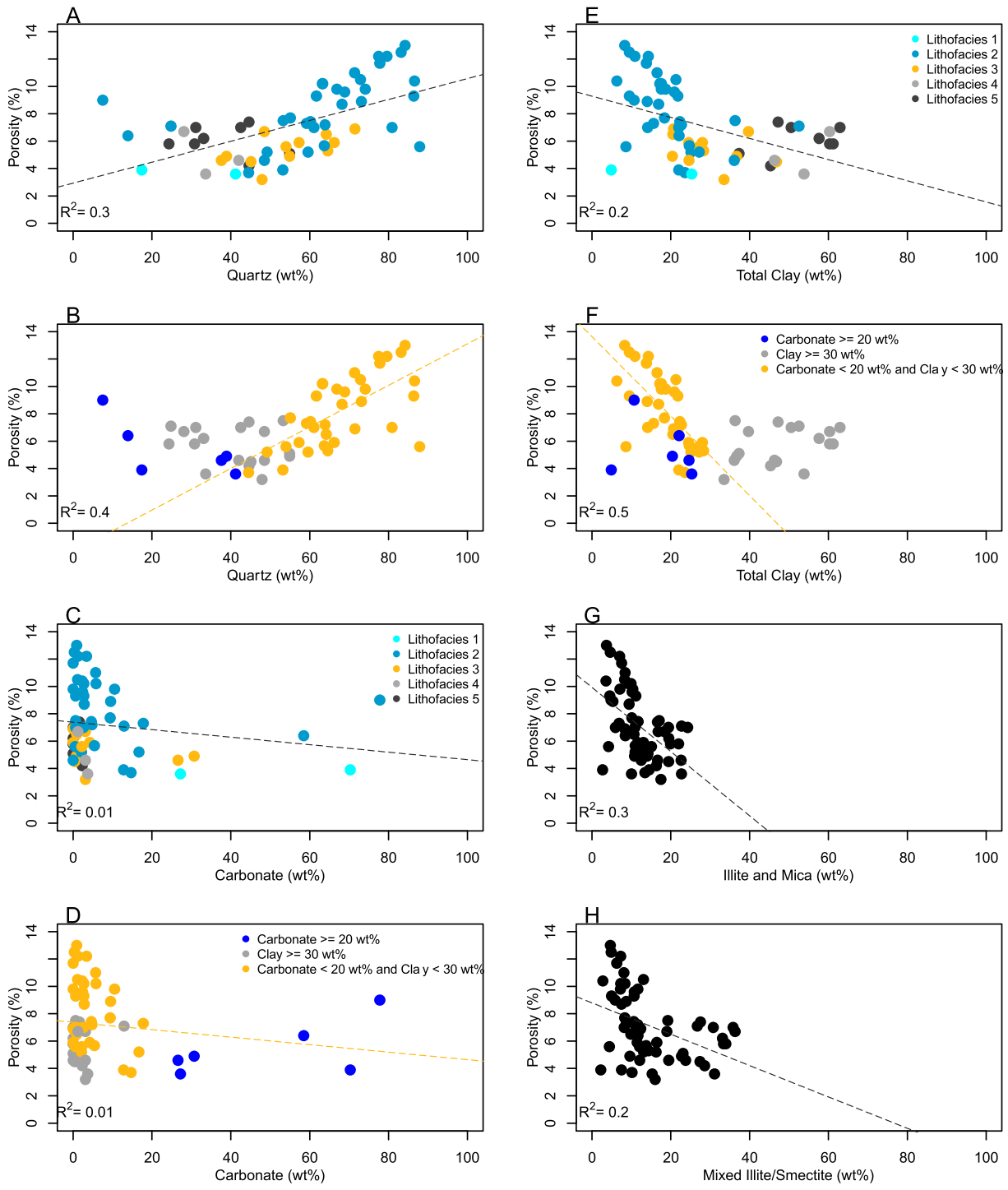

Fig. 18. Cross-plots of mineralogy and depth with porosity. (A) quartz–porosity colour coded by lithofacies, (B) quartz–porosity colour-coded by mineralogy, (C) carbonate–porosity colour coded by lithofacies, (D) carbonate–porosity colour coded by mineralogy, (E) total clay– porosity colour coded by lithofacies, (F) total clay– porosity colour coded by mineralogy, (G) illite and mica–porosity, and (H) mixed illite/smectite. The linear regressions in (B) and (F) exclude samples with carbonate content exceeding 20 wt % and samples with clay content greater than 30 wt %. Porosity values are bulk porosity measurements calculated with the Gas Research Institute (GRI) method. Abbreviations: wt% – weight percent.
(For interpretation of the references to colour in this figure legend, the reader is referred to the Web version of this article.)

belonging entirely to Lithofacies 2 (Fig. 18 A and E). N_2 adsorption total pore volume also shows trends by lithofacies, with low total pore volume in both samples from Lithofacies 4 and 5, intermediate pore volume in both Lithofacies 3 samples (Fig. 14). However, Lithofacies 2 and 3 display variable pore volume (Fig. 14). Compared to the mineralogical data (Fig. 6 A), it seems that the trends in porosity associated with each lithofacies (Fig. 8 A) can largely be explained by the respective proportions of quartz and clay. Additionally, macro-scale fractures in this interval are lithofacies-dependent, which is likely also controlled by the relative abundance of quartz, clay, and carbonate in each lithofacies, with fractures observed in the more quartz- or carbonate-rich Lithofacies 1–3, but an absence of fractures in Lithofacies 4 and 5 probably due to the higher clay content associated with these intervals.

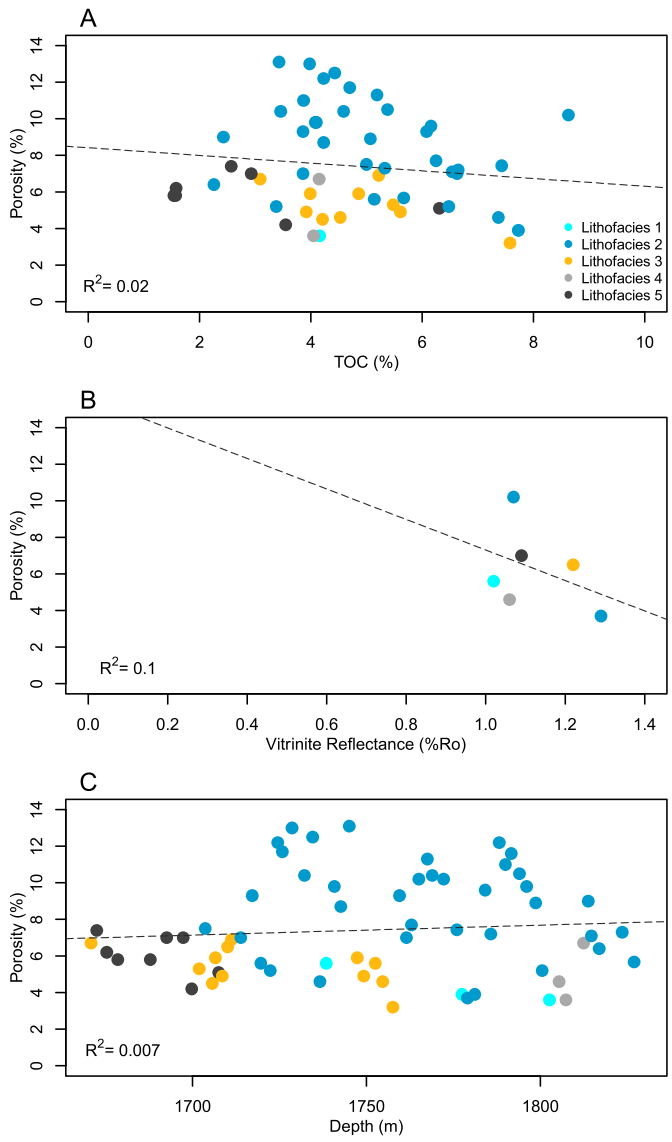

Fig. 19. Crossplots of (A) TOC–porosity coloured by lithofacies, (B) vitrinite reflectance– porosity coloured by lithofacies, and (C) depth–porosity by lithofacies. Porosity values are bulk porosity measurements calculated with the Gas Research Institute (GRI) method. Definitions: $\%R_o$ – percentage reflectance in oil immersion. (For interpretation of the references to colour in this figure legend, the reader is referred to the Web version of this article.)

5.3. Comparison to other fine-grained unconventional reservoirs

Mineralogically, the Canol Formation falls into the high end of quartz and feldspar content compared to other unconventional reservoirs and is most similar to the Devonian Muskwa Formation of the Horn River Group in British Columbia (Fig. 20). The Bluefish Member has levels of quartz and feldspar comparable to other fine-grained unconventional plays, with carbonate content more similar to the Eagle Ford of south Texas (Fig. 20). In contrast, the Bell Creek Member of the Hare Indian Formation has significantly higher clay content than the other organic-rich mudstone intervals considered (Fig. 20). Relative to the other units considered, Lithofacies 2 and 3 show high quartz and feldspar and plot near the average for the Canol Formation (Fig. 20). Lithofacies 1 has higher carbonate content than the Bluefish Member average and plots close to the Eagle Ford Formation and the Evie Member of the Horn River Formation of British Columbia (Fig. 20). Lithofacies 4 and 5 are more clay-rich than all other units considered (Fig. 20).

Average bulk porosities of the Hare Indian and Canol Formations are similar to bulk porosities of other organic-rich mudstone plays from the literature, with the Canol Formation, Bluefish Member, and Lithofacies 2 plotting amongst the highest average porosities (Fig. 21A). Nonetheless, compared to the samples from the fine-grained intervals analyzed in Clarkson et al. (2013), all the N-09 core samples plot at the low end of N_2 pore volume (Fig. 21B). This may be explained by a lower proportion of mesopores in the N-09 core samples than the other fine-grained examples considered.

Pore type in the Horn River Group of the N-09 core differs from many other mudstone reservoirs. For example, intervals with a dominance of organic-hosted porosity include the Barnett Shale (Curtis et al., 2012b; Loucks et al., 2012), the Woodford Formation (Curtis et al., 2012b), the Marcellus Formation (Milliken et al., 2013), the Horn River Group of British Columbia (Dong et al., 2015), and the oil- and gas-window samples of the Duvernay Formation (Dong et al., 2020). Our results suggest that the pore network in the Horn River Group is more

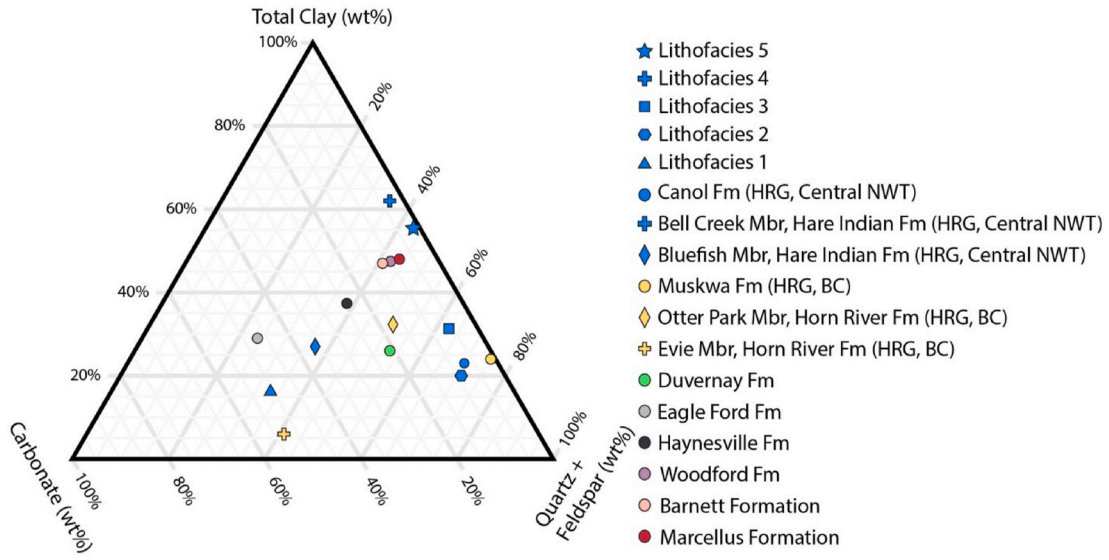

Fig. 20. Ternary diagram illustrating the mineralogy of several fine-grained unconventional resource plays in North America relative to the units in the Horn River Group of the N-09 core (NWT). Total clay, quartz and feldspar, and carbonate (calcite and dolomite) abundance have been normalized to 100%. Horn River Group BC data from Dong et al. (2017), Duvernay data from Ghanizadeh et al. (2015), Yassin et al. (2017), and Yassin et al. (2018), Eagle Ford data from Jennings and Antia (2013), Barnett data from Loucks et al. (2009) and Chalmers et al. (2012), Marcellus data from Milliken et al. (2013) and Chalmers et al. (2012), Woodford data from Chalmers et al. (2012), and Haynesville data from Klaver et al. (2015) and Chalmers et al. (2012). The data points are all averages and the data points from Lithofacies 1–5, the Canol Formation and the Hare Indian Formation are averages of the data presented herein. The same symbol is used for Lithofacies 4 and the Bell Creek Member of the Hare Indian Formation because the data points for both plot in the same area. Acronyms: BC – British Columbia, HRG – Horn River Group, NWT – Northwest Territories.
(For interpretation of the references to colour in this figure legend, the reader is referred to the Web version of this article.)

comparable to units that are not dominated by organic matter porosity. For example, the Bossier Formation displays dominantly intraparticle porosity (Loucks et al., 2012), intervals such as the Eagle Ford (Curtis et al., 2012b; Jennings and Antia, 2013) and the Kimmeridge Clay (Fishman et al., 2012) have mixed pore networks, and the Lower Cretaceous Pearsall Formation mudstone comprises primarily interparticle pores (Loucks et al., 2012).

5.4. Significance to reservoir potential

Quartz increases brittleness in sedimentary rocks, with biogenic silica further increasing hardness because it produces an interconnected silica cement framework through recrystallization (Liu et al., 2020). Thus, the high quartz and biogenic silica content of the Bluefish Member and Canol Formation, and specifically Lithofacies 2 and 3, is favourable for hydraulic fracture propagation. Natural fractures may enhance production (e.g., the Eagle Ford Formation; Aguilera and Ramirez Vargas, 2016) by serving as pathways for hydrocarbon movement to mechanical fractures or to the wellbore (Gale et al., 2007; Löhr et al., 2015). This may prove to be the case for Horn River Group Lithofacies 1, 2, and 3. For intervals with pervasive and interconnected organic matter pores, it has been suggested, although not confirmed, that this network may also act as a hydrocarbon flow pathway to induced fractures (e.g., Loucks et al., 2009; Curtis et al., 2012b). This potential flow pathway through organic matter pores is not present in the Horn River Group of the N-09 core.

The prevalent pore type also has implications for wettability. It has been suggested that organic pores are hydrocarbon wet, whereas mineral matrix pores may be hydrophilic or mixed (e.g., Bennett et al., 2004; Aplin and Larter, 2005; Aplin and Macquaker, 2011; Curtis et al., 2012b). Recent work indicates that thermal maturity also influences this relationship, and results showed that organic matter wettability changes from water-wet at low thermal maturities to oil-wet at high thermal maturities (e.g., Hu et al., 2016; Yassin et al., 2017; Jagadisan and Heidari, 2019; Begum et al., 2019). Accordingly, based on the thermal maturity of the samples, the organic matter pores in the N-09 core are likely somewhere in the middle of this spectrum (possibly mixed or oil-wet). However, a significantly greater proportion of interparticle pores compared to organic matter pores in the Horn River Group of the N-09 core could mean that overall, pores are primarily water-wet or mixed.

6. Conclusions

Porosity in the Devonian Horn River Group and lowermost Imperial Formation was assessed using a dataset comprising GRI porosity, TOC, XRD, vitrinite reflectance, Rock-Eval pyrolysis, SEM images, N_2 adsorption pore volume and pore size distribution, and lithofacies analysis from the Husky Little Bear N-09 core in the Central Mackenzie Valley of the NWT. The following key insights stem from our results:

(1) Interparticle pores, intraparticle pores and organic matter pores are all observed in the studied samples. Pores observed with SEM are irregular or slit-like, whereas the shape of hysteresis loops from N_2 porosimetry is suggestive of a slit-like shape. This difference is attributed to the difference in scale between the pores observed with SEM (mostly macropores) versus those included in N_2 results (mesopores). A lack of TOC-porosity correlation suggests that mineral matrix pores (interparticle and/or intraparticle) are dominant relative to organic matter pores.
(2) For all samples considered, the highest pore volume is hosted by mesopores with a radius of approximately 2 nm, which are interpreted to be mineral matrix pores because of the absence of a positive TOC-porosity relationship.
(3) Mineralogy (particularly quartz and total clay abundance) is the best predictor of porosity in this interval. Trends in porosity associated with the lithofacies are also apparent and Lithofacies 2 is characterized by the highest mean porosity. The lithofacies-porosity trends are attributed to the differences in mineralogy between the lithofacies.

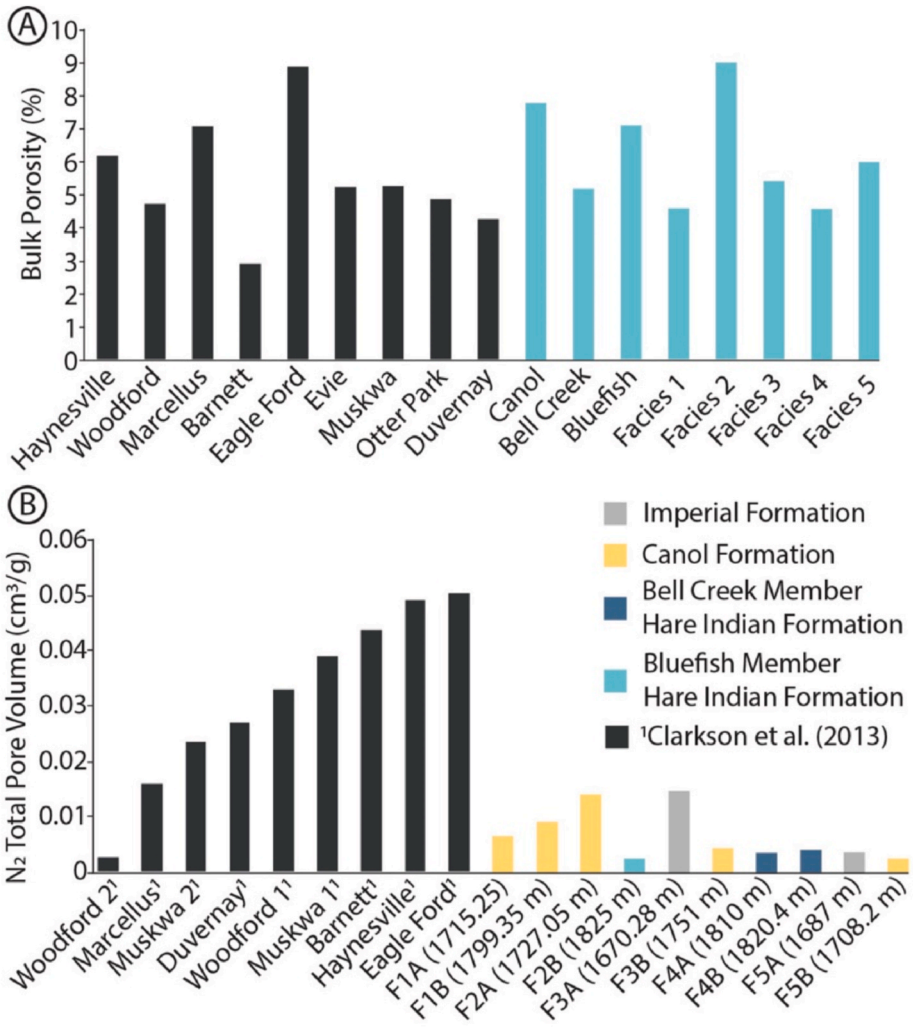

Fig. 21. Comparison of porosity values for the Horn River Group and lower Imperial Formation of the N-09 core to those from other North American mudstone plays. (A) Comparison to bulk porosity data (Gas Research Institute method, from Hg intrusion and He pycnometry) from other fine-grained North American unconventional plays. The Evie, Muskwa, and Otter Park results are averages from Dong et al. (2017), the Duvernay results are an average of the data from Ghanizadeh et al. (2015), Yassin et al. (2017), and Yassin et al. (2018), the Eagle Ford results are an average of the data presented in Jennings and Antia (2013), the Barnett results are an average of the data presented in Loucks et al. (2009) and Chalmers et al. (2012), the Marcellus results are an average of the data presented in Milliken et al. (2013) and Chalmers et al. (2012), the Woodford results are from Chalmers et al. (2012), and the Haynesville results are from Chalmers et al. (2012). The data bars for Lithofacies 1–5, the Canol, the Bluefish, and the Bell Creek are averages of the dataset presented herein. (B) Nitrogen porosimetry pore volumes from the Horn River Group relative to nitrogen porosimetry pore volumes from other unconventional reservoirs. Modified from Clarkson et al. (2013).
(For interpretation of the references to colour in this figure legend, the reader is referred to the Web version of this article.)

(4) Relative to other North American mudstone reservoirs, the Bluefish and Canol Formations, and particularly Lithofacies 2 and 3, plot amongst the units with the highest quartz + feldspar content and have comparable bulk porosity, although lower mesopore volume. In terms of primary pore type, the Horn River Group differs from organic matter pore-dominated units such as the Barnett Shale, Woodford Formation, Marcellus Formation, and Horn River Group of British Columbia.
(5) The Bluefish Member and Canol Formation are favourable prospects for hydraulic fracturing. Moreover, natural fractures may facilitate the movement of hydrocarbons to mechanical fractures. Nevertheless, these intervals appear to lack the interconnected network of organic matter pores that characterizes many other unconventional mudstone reservoirs. Although they lack this organic pore network, the Bluefish Member and the Canol Formation may be mixed-wet or water-wet compared to other such units.

These results further elucidate the character and distribution of prospective reservoir units in the Horn River Group of the NWT. Moreover, our findings will facilitate the prediction and modeling of hydrocarbon potential in the frontier Northern Canadian Mainland Sedimentary Basin. Finally, this work contributes to our understanding of porosity types, properties, and controls in highly siliceous mudstone lithologies, unique relative to most other fine-grained North American reservoirs.

Declaration of competing interest

The authors declare that they have no known competing financial interests or personal relationships that could have appeared to influence the work reported in this paper.

Acknowledgements

We thank Husky Energy and particularly Dave Herbers for providing us with this core and associated GRI porosity, TOC, XRD, vitrinite reflectance, and Rock-Eval pyroallysis datasets. We are also grateful to Dr. Nancy Zhang from the nanoFAB facility at the University of Alberta for training and guidance with N_2 porosimetry, Carolyn Currie of Core Laboratories Canada Ltd. for providing guidance and clarification about methods, and Smriti Dhiman for her help with multivariate statistics. Thank you to the the Northwest Territories Geological Survey, the SEPM Foundation, and the NSERC Discovery Grant to MKG for funding this project. Finally, we thank the editor, Dr. Bo Liu, for the handling of this manuscript and the three anonymous reviewers for constructive feedback.

Appendix A. Supplementary data

Supplementary data to this article can be found online at https://doi.org/10.1016/j.marpetgeo.2022.105738.

References

Abdi, H., Valenti, D., 2007. Multiple correspondence analysis. In: Salkind, N.J. (Ed.), Encyclopedia of Measurement and Statistics. Sage Publications, Thousand Oaks (CA, pp. 652–657, 10.4135/9781412952644.

Abdi, H., Williams, L.J., 2010. Principal component analysis. Wiley Interdisciplinary Reviews: Comput. Stat. 2 (4), 433–459, 10.1002/wics.101.

Aguilera, R., Ramirez Vargas, J.F., 2016. Factors controlling fluid migration and distribution in the Eagle Ford shale. SPE Reservoir Eval. Eng. 19 (3), 403–414, 10.2118/171626-PA.

Al-Aasm, I.S., Morad, S., Durocher, S., Muir, I., 1996. Sedimentology, C–S–Fe relationships and stable isotopic compositions in Devonian black mudrocks, Mackenzie Mountains, Northwest Territories, Canada. Sediment. Geol. 106, 279–298. https://doi.org/10.1016/S0037-0738(96)00018-8.

Ambrose, R.J., Hartman, R.C., Diaz-Campos, M., Akkutlu, I.Y., Sondergeld, C.H., 2010. New pore-scale considerations for shale gas in place calculations: society of petroleum engineers unconventional gas conference. Pittsburgh, Pennsylvania. February 23–25, 2010, SPE Paper 131772, 17 pp., doi:10.2118/131772-MS.

Aplin, A.C., Larter, S.R., 2005. Fluid flow, pore pressure, wettability, and leakage in mudstone cap rocks. In: Boult, P., Kaldi, J. (Eds.), Evaluating Fault and Cap Rock Seals: AAPG Hedberg Series 2, pp. 1–12.

Aplin, A.C., Macquaker, J.H.S., 2011. Mudstone diversity: origin and implications for source, seal, and reservoir properties in petroleum systems. AAPG (Am. Assoc. Pet. Geol.) Bull. 95, 2031–2059, 10.1306/03281110162.

Begum, M., Yassin, M.R., Dehghanpour, H., 2019. Effect of kerogen maturity on organic shale wettability: a Duvernay case study. Mar. Petrol. Geol. 110, 483–496. https://doi.org/10.1016/j.marpetgeo.2019.07.012.

Bennett, B., Buckman, J.O., Bowler, B.F.J., Larter, S.R., 2004. Wettability alteration in petroleum systems: the role of polar nonhydrocarbons. Petrol. Geosci. 10, 271–277, 10.1144/1354-079303-606.

Beranek, L.P., Mortensen, J.K., Lane, L.S., Allen, T.L., Fraser, T.A., Hadlari, T., Zantvoort, W.G., 2010. Detrital zircon geochronology of the western Ellesmerian clastic wedge, northwestern Canada: insights on Arctic tectonics and the evolution of the northern Cordilleran miogeocline. GSA Bulletin 122 (11/12), 1899–1911, 10.1130/B30120.1.

Bertrand, R., 1990. Correlations among the reflectances of vitrinite, chitinozoans, graptolites and scolecodonts. Org. Geochem. 15 (6), 565–574. https://doi.org/10.1016/0146-6380(90)90102-6.

Biddle, S.K., LaGrange, M.T., Harris, B.S., Fiess, K., Terlaky, V., Gingras, M.K., 2021. A fine detail physiochemical depositional model for Devonian organic-rich mudstones: a petrographic study of the Hare Indian and Canol formations, Central Mackenzie Valley, Northwest Territories. Sediment. Geol. 414, 105838, 10.1016/j.sedgeo.2020.105838.

Brunauer, S., Emmett, P.H., Teller, E., 1938. Adsorption of gases in multimolecular layers. J. Am. Chem. Soc. 60 (2), 309–319. https://doi.org/10.1021/ja01269a023.

Canter, L., Zhang, S., Sonnenfeld, M., Bugge, C., Guisinger, M., Jones, K., 2016. Primary and secondary organic matter habit in unconventional reservoirs. In: Olson, T. (Ed.), Imaging Unconventional Reservoir Pore Systems: AAPG Memoir 112, pp. 9–24, 10.1306/13592014M1123691.

Carr, A.D., 2000. Suppression and retardation of vitrinite reflectance, part 1. Formation and significance for hydrocarbon generation. J. Petrol. Geol. 23 (3), 313–343, 10.1111/j.1747-5457.2000.tb01022.x.

Chalmers, G.R., Bustin, R.M., Power, I.M., 2012. Characterization of gas shale pore systems by porosimetry, pycnometry, surface area, and field emission scanning electron microscopy/transmission electron microscopy image analyses: examples from the Barnett, Woodford, Haynesville, Marcellus, and Doig units. AAPG (Am. Assoc. Pet. Geol.) Bull. 96 (6), 1099–1119.

Chavent, M., Kuentz-Simonet, V., Labenne, A., Saracco, J., 2015. Multivariate Analysis of Mixed Data: the PCAmixdata R Package arXiv:1411.4911v3 [stat.CO] 4 Dec 2014.

Chen, Z., Wang, T., Liu, Q., Zhang, S., Zhang, L., 2015. Quantitative evaluation of potential organic-matter porosity and hydrocarbon generation and expulsion from mudstone in continental lake basins: a case study of Dongying sag, eastern China. Mar. Petrol. Geol. 66, 906–924. https://doi.org/10.1016/j.marpetgeo.2015.07.027.

Clarkson, C.R., Solano, N., Bustin, R.M., Bustin, A.M.M., Chalmers, G.R.L., He, L., Melnichenko, Y.B., Radlinski, A.P., Blach, T.P., 2013. Pore structure characterization of North American shale gas reservoirs using USANS/SANS, gas adsorption, and mercury intrusion. Fuel 103, 606–616. https://doi.org/10.1016/j.fuel.2012.06.119.

Curtis, M.E., Cardott, B.J., Sondergeld, C.H., Rai, C.S., 2012a. Development of organic porosity in the Woodford Shale with increasing thermal maturity. Int. J. Coal Geol. 103, 26–31. https://doi.org/10.1016/j.coal.2012.08.004.

Curtis, M.E., Sondergeld, C.H., Ambrose, R.J., Rai, C.S., 2012b. Microstructural investigation of gas shales in two and three dimensions using nanometer-scale resolution imaging. AAPG (Am. Assoc. Pet. Geol.) Bull. 96 (4), 665–677, 10.1306/08151110188.

Dembicki Jr., H., 2009. Three common source rock evaluation errors made by geologists during prospect or play appraisals. AAPG (Am. Assoc. Pet. Geol.) Bull. 93 (3), 341–356, 10.1306/10230808076.

Dewing, K., Hadlari, T., Pearson, D.G., Matthews, W., 2019. Early ordovician to early devonian tectonic development of the northern margin of Laurentia, Canadian arctic islands. GSA Bulletin 131 (7/8), 1075–1094, 10.1130/B35017.1.

Dong, T., Harris, N.B., Ayranci, K., Twemlow, C.E., Nassichuk, B.R., 2015. Porosity characteristics of the Devonian Horn River shale, Canada: insights from lithofacies classification and shale composition. Int. J. Coal Geol. 141–142, 74–90. https://doi.org/10.1016/j.coal.2015.03.001.

Dong, T., Harris, N.B., Ayranci, K., Twemlow, C.E., Nassichuk, B.R., 2017. The impact of composition on pore throat size and permeability in high maturity shales: middle and Upper Devonian Horn River Group, northeastern British Columbia, Canada. Mar. Petrol. Geol. 81, 220–236. https://doi.org/10.1016/j.marpetgeo.2017.01.011.

Dong, T., Harris, N.B., McMillan, J.M., Twemlow, C.E., Nassichuk, B.R., Bish, D.L., 2019. A model for porosity evolution in shale reservoirs: an example from the Upper Devonian Duvernay Formation. West. Canada Sediment. Basin: AAPG (Am. Assoc. Pet. Geol.) Bull. 103 (5), 1017–1044, 10.1306/10261817272.

Dong, T., Harris, N.B., McMillan, J.M., Twemlow, C.E., Nassichuk, B.R., Bish, D.L., 2020. A model for porosity evolution in shale reservoirs: an example from the Upper Devonian Duvernay Formation. West. Canad. Sediment. Basin: AAPG (Am. Assoc. Pet. Geol.) Bull. 103 (5), 1017–1044, 10.1306/10261817272.

Egenhoff, S.O., Fishman, N.S., 2013. Traces in the dark—sedimentary processes and facies gradients in the upper shale member of the upper devonian–lower mississippian bakken formation, williston basin, North Dakota, USA. J. Sediment. Res. 83 (9), 803–824, 10.2110/jsr.2013.60.

El Attar, A., Pranter, M.J., 2016. Regional stratigraphy, elemental chemostratigraphy, and organic richness of the Niobrara Member of the Mancos Shale. Piceance Basin, Colorado: AAPG (Am. Assoc. Pet. Geol.) Bull. 100 (3), 345–377, 10.1306/12071514127.

Emmanuel, S., Day-Stirrat, R.J., 2012. A framework for quantifying size dependent deformation of nano-scale pores in mudrocks. J. Appl. Geophys. 86, 29–35. https://doi.org/10.1016/j.jappgeo.2012.07.011.

Espitalié, J., Deroo, G., Marquis, F., 1985. Rock-eval pyrolysis and its applications. Rev. Inst. Fr. Petrol 40 (5), 563–579.

Fermont, W.J.J., 1988. Possible causes of abnormal vitrinite reflectance values in paralic deposits of the Carboniferous in the Achterhoek area. The Netherlanks: Org. Geochem. 12 (4), 401–411. https://doi.org/10.1016/0146-6380(88)90013-7.

Fishman, N.S., Hackley, P.C., Lowers, H.A., Hill, R.J., Egenhoff, S.O., Eberl, D.E., Blum, A.E., 2012. The nature of porosity in organic-rich mudstones of the upper jurassic Kimmeridge Clay Formation, North Sea, offshore United Kingdom. Int. J. Coal Geol. 103, 32–50. https://doi.org/10.1016/j.coal.2012.07.012.

Fraser, T.A., Hutchison, M.P., 2017. Lithogeochemical characterization of the middle–upper devonian road River Group and Canol and imperial formations on trail river, east Richardson Mountains, Yukon: age constraints and a depositional model for fine-grained strata in the lower paleozoic Richardson Trough. Can. J. Earth Sci. 54 (7), 731–765, 10.1139/cjes-2016-0216.

Fritz, W.H., Cecile, M.P., Norford, B.S., Morrow, D., Geldsetzer, H.H.J., 1991. Cambrian to middle devonian assemblages. In: Gabrielse, H., Yorath, C.J. (Eds.), Geol. Cordilleran Orogen Canada: Geol. Surv. Canada, Geol. Canada 4, 151–218.

Gale, J.F., Reed, R.M., Holder, J., 2007. Natural fractures in the Barnett Shale and their importance for hydraulic fracture treatments. AAPG Bull. 91 (4), 603–622, 10.1306/11010606061.

Garzione, C.N., Patchett, P.J., Ross, G.M., Nelson, J., 1997. Provenance of Paleozoic sedimentary rocks in the Canadian Cordilleran miogeocline: a Nd isotopic study. Can. J. Earth Sci. 34 (12), 1603–1618, 10.1139/e17-129.

Ghanizadeh, A., Bhowmik, S., Haeri-Ardakani, O., Sanei, H., Clarkson, C.R., 2015. A comparison of shale permeability coefficients derived using multiple non-steady-state measurement techniques: examples from the Duvernay Formation, Alberta (Canada). Fuel 140, 371–387. https://doi.org/10.1016/j.fuel.2014.09.073.

Hadlari, T., 2015. Oil migration driven by exhumation of the Canol Formation oil shale: a new conceptual model for the Norman Wells oil field, northwestern Canada. Mar. Petrol. Geol. 65, 172–177. https://doi.org/10.1016/j.marpetgeo.2015.03.027.

Hadlari, T., Davis, W.J., Dewing, K., 2014a. A pericratonic model for the Pearya terrane as an extension of the Franklinian margin of Laurentia. Canadian Arctic: GSA Bulletin 126 (1/2), 182–200, 10.1130/B30843.1.

Hadlari, T., MacLean, B.C., Galloway, J.M., Sweet, A.R., White, J.M., Thomson, D., Gabites, J., Schröder-Adams, C.J., 2014b. The flexural margin, the foredeep, and the orogenic margin of a northern Cordilleran foreland basin: Cretaceous tectonostratigraphy and detrital zircon provenance, northwestern Canada. Mar. Petrol. Geol. 57, 173–186, 10.1016/j.marpetgeo.2014.05.019.

Hadlari, T., MacLean, B.C., Pyle, L.J., Fallas, K.M., Durbano, A.M., 2015. A Combined Depth and Thermal Maturity Map of the Canol Formation, Northern Mackenzie Valley, Northwest Territories. Geological Survey of Canada. Open File 7865, doi:10.4095/296460.

Han, C., Jiang, Z., Han, M., Wu, M., Lin, W., 2016. The lithofacies and reservoir characteristics of the upper ordovician and lower silurian black shale in the southern Sichuan Basin and its periphery, China. Mar. Petrol. Geol. 75, 181–191. https://doi.org/10.1016/j.marpetgeo.2016.04.014.

Harris, B.S., LaGrange, M.T., Biddle, S.K., Playter, T.L., Fiess, K.M., Gingras, M.K., 2022. Chemostratigraphy of the fine-grained Hare Indian Formation in the Mackenzie Mountains and central Mackenzie Valley, Northwest Territories, Canada. Can. J. Earth Sci. 59 (1), 29–45, 10.1139/cjes-2020-0198.

Hover, V.C., Peacor, D.R., Walter, L.M., 1996. STEM/AEM evidence for preservation of burial diagenetic fabrics in Devonian shales; implications for fluid/rock interaction in cratonic basins (USA). J. Sediment. Res. 66 (3), 519–530, 10.1306/D4268397-2B26-11D7-8648000102C1865D.

Hower, J., Eslinger, E.V., Hower, M.E., Perry, E.A., 1976. Mechanism of burial metamorphism of argillaceous sediment: 1. Mineralogical and chemical evidence. GSA Bulletin 87 (5), 725–737, 10.1130/0016-7606(1976)87<725:MOBMOA>2.0.CO;2.

Hu, Y., Devegowda, D., Sigal, R., 2016. A microscopic characterization of wettability in shale kerogen with varying maturity levels. J. Nat. Gas Sci. Eng. 33, 1078–1086. https://doi.org/10.1016/j.jngse.2016.06.014.

Irish, J.P.R., Kempthorne, R.H., 1987. The study of natural fractures in a reef complex, Norma Wells Oilfield, Canada. In: Tillman, R.W., Weber, K.J. (Eds.), Res. Sedimentol.: Soc. Econ. Paleontol. Mineral. Spec. Publ. 40, 153–168, 10.2110/pec.87.40.0153.

Issler, D.R., Grist, A.M., Stasiuk, L.D., 2005. Post-Early Devonian thermal constraints on hydrocarbon source rock maturation in the Keele Tectonic Zone, Tulita area, NWT, Canada, from multi-kinetic apatite fission track thermochronology, vitrinite reflectance and shale compaction. Bull. Can. Petrol. Geol. 53 (4), 405–431, 10.2113/53.4.405.

Jagadisan, A., Heidari, Z., 2019. Experimental quantification of the effect of thermal maturity of kerogen on its wettability. SPE Reservoir Eval. Eng. 22 (4), 1323–1333, 10.2118/195684-PA.

James, G., Witten, D., Hastie, T., Tibshirani, R., 2013. An Introduction to Statistical Learning with Applications in R. Springer, New York, p. 426.

Jeletzky, J.A., 1975. Jurassic and Lower Cretaceous Paleogeography and Depositional Tectonics of Porcupine Plateau, Adjacent Areas of Northern Yukon and Those of Mackenzie District: Geological Survey of Canada. Paper 74-16, p. 52. doi:10.4095/102549.

Jennings, D.S., Antia, J., 2013. Petrographic characterization of the Eagle Ford shale, south Texas: mineralogy, common constituents, and distribution of nanometer-scale pore types. In: Camp, W., Diaz, E., Wawak, B. (Eds.), Electron Microscopy of Shale Hydrocarbon Reservoirs: AAPG Memoir 102, pp. 101–113, 10.1306/13391708M1023586.

Kabanov, P., 2019. Devonian (c. 388–375 Ma) Horn River Group of Mackenzie Platform (NW Canada) is an open-shelf succession recording oceanic anoxic events. J. Geol. Soc. 176 (1), 29–45, 10.1144/jgs2018-075.

Kabanov, P., Deblonde, C., 2019. Geological and geochemical data from Mackenzie Corridor. Part VIII: middle-Upper Devonian lithostratigraphy, formation tops, and isopach maps in NTS areas 96 and 106, Northwest Territories and Yukon. Open File 8552 Geol. Surv. Canada 39, 10.4095/314785.

Kabanov, P., Gouwy, S.A., 2017. The Devonian Horn River Group and the basal Imperial Formation of the central Mackenzie Plain, NWT, Canada: multiproxy stratigraphic framework of a black shale basin. Can. J. Earth Sci. 54 (4), 409–429, 10.1139/cjes-2016-0096.

Kabanov, P., Jiang, C., 2020. Photic-zone euxinia and anoxic events in a Middle-Late Devonian shelfal sea of Panthalassan continental margin, NW Canada: changing paradigm of Devonian ocean and sea level fluctuations. Global Planet. Change 103153, 1–19, 10.1016/j.gloplacha.2020.103153.

Katz, B.J., Arango, I., 2018. Organic porosity: a geochemist's view of the current state of understanding. Org. Geochem. 123, 1–16. https://doi.org/10.1016/j.orggeochem.2018.05.015.

Keller, L.M., Holzer, L., Wepf, R., Gasser, P., Münch, B., Marschall, P., 2011. On the application of focused ion beam nanotomography in characterizing the 3D pore space geometry of Opalinus clay. Phys. Chem. Earth 36, 1539–1544. https://doi.org/10.1016/j.pce.2011.07.010. Parts A/B/C.

Keller, M.A., Isaacs, C.M., 1985. An evaluation of temperature scales for silica diagenesis in diatomaceous sequences including a new approach based on the Miocene Monterey Formation. California: Geo Mar. Lett. 5 (1), 31–35, 10.1007/BF02629794.

Klaver, J., Desbois, G., Littke, R., Urai, J., 2015. BIB-SEM characterization of pore space morphology and distribution in postmature to overmature samples from the Haynesville and Bossier Shales. Mar. Petrol. Geol. 59, 451–466, 10.1016/j.marpetgeo.2014.09.020.

Klaver, J., Desbois, G., Littke, R., Urai, J., 2016. BIB-SEM pore characterization of mature and post mature Posidonia Shale samples from the Hils area, Germany. Int. J. Coal Geol. 158, 78–89. https://doi.org/10.1016/j.coal.2016.03.003.

Knapp, L.J., Ardakani, O.H., Uchida, S., Nanjo, T., Otomo, C., Hattori, T., 2020. The influence of rigid matrix minerals on organic porosity and pore size in shale reservoirs: upper Devonian Duvernay Formation, Alberta, Canada. Int. J. Coal Geol. 227, 103525. https://doi.org/10.1016/j.coal.2020.103525.

Konhauser, K.O., 2007. Introduction to Geomicrobiology. Blackwell, Malden, Massachusetts.

Law, C.A., 1999. Evaluating source rocks. In: Beaumont, A.E., Foster, N.H. (Eds.), Treatise of Petroleum Geology/Handbook of Petroleum Geology: Exploring for Oil and Gas Traps. AAPG Special Bulletin, pp. 1–41 (Chapter 6).

Lazar, O.R., Bohacs, K.M., Macquaker, J.H.S., Schiber, J., Demko, T., 2015. Capturing key attributes of fine-grained sedimentary rocks in outcrops, cores, and thin sections: nomenclatures and description guidelines. J. Sediment. Res. 85, 230–246, 10.2110/jsr.2015.11.

Lenz, A.C., 1972. Ordovician to devonian history of northern Yukon and adjacent district of Mackenzie. Bull. Can. Petrol. Geol. 20 (2), 321–361, 10.35767/gscpgbull.20.2.321.

Li, J., Ma, Y., Huang, K., Zhang, Y., Wang, W., Liu, J., Li, Z., Lu, S., 2018a. Quantitative characterization of organic acid generation, decarboxylation, and dissolution in a shale reservoir and the corresponding applications—a case study of the Bohai Bay Basin. Fuel 214, 538–545, 10.1016/j.fuel.2017.11.034.

Li, Y., Schieber, J., Fan, T., Wei, X., 2018b. Pore characterization and shale facies analysis of the Ordovician-Silurian transition of northern Guizhou, South China: the controls of shale facies on pore distribution. Mar. Petrol. Geol. 92, 697–718. https://doi.org/10.1016/j.marpetgeo.2017.12.001.

Liu, B., Schieber, J., Mastalerz, M., Teng, J., 2020. Variability of rock mechanical properties in the sequence stratigraphic context of the upper devonian new albany shale, Illinois basin. Mar. Petrol. Geol. 112, 104068. https://doi.org/10.1016/j.marpetgeo.2019.104068.

Löhr, S.C., Baruch, E.T., Hall, P.A., Kennedy, M.J., 2015. Is organic pore development in gas shales influenced by the primary porosity and structure of thermally immature organic matter. Org. Geochem. 87, 119–132. https://doi.org/10.1016/j.orggeochem.2015.07.010.

Loucks, R.G., Reed, R.M., 2014. Scanning-Electron-Microscope petrographic evidence for distinguishing organic-matter pores associated with depositional organic matter versus migrated organic matter in mudrocks. Gulf Coast Ass. Geol. Soc. J. 3, 51–60.

Loucks, R.G., Reed, R.M., Ruppel, S.C., Hammes, U., 2012. Spectrum of pore types and networks in mudrocks and descriptive classification for matrix-related mudrock pores. AAPG (Am. Assoc. Pet. Geol.) Bull. 96 (6), 1071–1098, 10.1306/08171111061.

Loucks, R.G., Reed, R.M., Ruppel, S.C., Jarvie, D.M., 2009. Morphology, genesis, and distribution of nanometer-scale pores in siliceous mudstones of the Mississippian Barnett Shale. J. Sediment. Res. 79, 848–861, 10.2110/jsr.2009.092.

Lu, J., Ruppel, S.C., Rowe, H.D., 2015. Organic matter pores and oil generation in the Tuscaloosa marine shale. AAPG (Am. Assoc. Pet. Geol.) Bull. 99 (2), 333–357, 10.1306/08201414055.

Luffel, D.L., Guidry, F.K., 1993. New core analysis methods for measuring reservoir rock properties of Devonian shale. J. Petrol. Technol. 44 (11), 1184–1190, 10.2118/20571-PA.

MacGowan, D.B., Surdam, R.C., 1990. Carboxylic acid anions in formation waters, san joaquin basin and Louisiana Gulf coast, USA—implications for clastic diagenesis. Appl. Geochem. 5 (5–6), 687–701, 10.1016/0883-2927(90)90065-D.

MacKenzie, W.S., 1974. Radiolaria from the Canol Formation, Northwest Territories. Geological Survey of Canada. Paper 74-1, Part A, 396 pp., doi:10.4095/103272.

MacLean, B.C., 2011. Tectonic and stratigraphic evolution of the Cambrian basin of northern Northwest Territories. Bull. Can. Petrol. Geol. 59 (2), 172–194, 10.2113/gscpgbull.59.2.172.

MacLean, B.C., Fallas, K.M., Hadlari, T., 2014. The multi-phase keele arch, central Mackenzie corridor, Northwest Territories. Bull. Can. Petrol. Geol. 62 (2), 68–104, 10.2113/gscpgbull.62.2.68.

MacNeil, A.J., Jones, B., 2006. Ovummuridae (calcareous microfossils) from a Late Devonian ramp: their distribution, preservation potential, and paleoecological significance. Can. J. Earth Sci. 43, 269–280, 10.1139/e05-105.

Macquaker, J.H., Taylor, K.G., Keller, M., Polya, D., 2014. Compositional controls on early diagenetic pathways in fine-grained sedimentary rocks: implications for predicting unconventional reservoir attributes of mudstones. AAPG (Am. Assoc. Pet. Geol.) Bull. 98 (3), 587–603, 10.1306/08201311176.

Mastalerz, M., Schimmelmann, A., Drobniack, A., Chen, Y., 2013. Porosity of Devonian and Mississippian New Albany Shale across a maturation gradient: insights from organic petrology, gas adsorption, and mercury intrusion. AAPG (Am. Assoc. Pet. Geol.) Bull. 97 (10), 1621–1643, 10.1306/04011312194.

Mazzotti, S., Hyndman, R.D., 2002. Yakutat collision and strain transfer across the northern Canadian Cordillera. Geology 30 (6), 495–498, 10.1130/0091-7613(2002)030<0495:YCASTA>2.0.CO;2.

Milliken, K.L., Curtis, M.E., 2016. Imaging pores in sedimentary rocks: foundation of porosity prediction. Mar. Petrol. Geol. 73, 590–608, 10.1016/j.marpetgeo.2016.03.020.

Milliken, K.L., Rudnicki, M., Awwiller, D.N., Zhang, T., 2013. Organic matter-hosted pore system. In: Marcellus Formation (Devonian), vol. 97. AAPG Bulletin, Pennsylvania, pp. 177–200, 10.1306/07231212048.

Morrow, D.W., 2018. Devonian of the northern Canadian mainland sedimentary basin: a review. Bull. Can. Petrol. Geol. 66 (3), 623–694.

Muir, I., Dixon, O.A., 1984. Facies analysis of a middle devonian sequence in the mountain river-gayna river. In: Brophy, J.A. (Ed.), Contributions to the Geology of the Northwest Territories, vol. 1, pp. 55–62.

Muir, I., Wong, P., Wendte, J., 1985. Devonian Hare Indian-Ramparts (Kee Scarp) Evolution, Mackenzie Mountains and Subsurface Norman Wells, NWT: Basin-Fill and Platform Reef Development: Society of Economic Paleontologists and Mineralogists (SEPM) Rocky Mountain Carbonate Reservoirs CW7, pp. 311–341.

Norris, A.W., 1985. Stratigraphy of Devonian Outcrop Belts in Northern Yukon Territory and Northwestern District of Mackenzie (Operation Porcupine Area). Memoir 410. Geological Survey of Canada, p. 81, 10.4095/120309.

Northwest Territories Geological Survey (NTGS) and National Energy Board (NEB), 2015. An Assessment of the Unconventional Petroleum Resources of the Bluefish Shale and the Canol Shale in the Northwest Territories - Energy Briefing Note. National Energy Board, Canada, p. 10.

Olivier, J.P., Conklin, W.B., Szombathely, M.v., 1994. In: Rouquerol, J., Rodriguez-Reinoso, F., Sing, K.S.W., Unger, K.K. (Eds.), Characterization of Porous Solids III, Studies in Surface Science and Catalysis, vol. 87, pp. 81–88.

Playter, T., Corlett, H., Konhauser, K., Robbins, L., Rohais, S., Crombez, V., Maccormack, K., Rokosh, D., Prenoslo, D., Furlong, C.M., Pawlowicz, J., Gingras, M., Lalonde, S., Lyster, S., Zonneveld, J.-P., 2018. Clinoform identification and correlation in fine-- grained sediments: a case study using the Triassic Montney Formation. Sedimentology 65 (1), 263–302.

Powell, J.W., Issler, D.R., Schneider, D.A., Fallas, K.M., Stockli, D.F., 2020. Thermal history of the Mackenzie plain, Northwest Territories, Canada: insights from low-temperature thermochronology of the devonian Imperial Formation. pp.3–4 GSA Bulletin v 132, 767–783, 10.1130/B35089.1.

Pugh, D.C., 1983. Pre-Mesozoic geology in the subsurface of Peel River map area. Memoir 401. In: Yukon Territory and District of Mackenzie. Geological Survey of Canada, p. 56, 10.4095/119498.

Pyle, L.J., Gal, L.P., Hadlari, T., 2015. Thermal Maturity Trends for Devonian Horn River Group Units and Equivalent Strata in the Mackenzie Corridor, Northwest Territories and Yukon: Geological Survey of Canada Open File Report No. 7850, 10.4095/296446.

Pyle, L.J., Gal, L.P., 2016. Reference section for the Horn River group and definition of the Bell Creek member, Hare Indian Formation in central Northwest Territories. Bull. Can. Petrol. Geol. 64 (1), 67–98, 10.2113/gscpgbull.64.1.67.

Ratcliffe, K.T., Wright, A.M., Schmidt, K., 2012. Application of inorganic whole-rock geochemistry to shale resource plays: an example from the Eagle Ford Shale Formation. Texas: Sediment. Rec. 10 (2), 4–9, 10.2110/sedred.2012.2.4.

Rock-Color Chart Committee, 2009. Geological Rock-Color Chart with Genuine Munsell Color Chips. Geological Society of America.
Ross, D.J.K., Bustin, M.R., 2009. The importance of shale composition and pore structure upon gas storage potential of shale gas reservoirs. Mar. Petrol. Geol. 26, 916–927, 10.1016/j.marpetgeo.2008.06.004.
Roychoudhury, A.N., Kostka, J.E., Van Cappellen, P., 2003. Pyritization: a palaeoenvironmental and redox proxy reevaluated: Estuarine. Coast. Shelf Sci. 57, 1183–1193, 10.1016/S0272-7714(03)00058-1.
Schieber, J., 2013. SEM observations on ion-milled samples of devonian black shales from Indiana and New York: the petrographic context of multiple pore types. In: Camp, W., Diaz, E., Wawak, B. (Eds.), Electron Microscopy of Shale Hydrocarbon Reservoirs: AAPG Memoir 102, pp. 153–171, 10.1306/13391711M1023589.
Schieber, J., Lazar, R., Bohacs, K., Klimentidis, R., Dumitrescu, M., Ottman, J., 2016. An SEM study of porosity in the Eagle Ford Shale of Texas—pore types and porosity distribution in a depositional and sequence-stratigraphic context. In: Breyer, J.A. (Ed.), The Eagle Ford Shale: A Renaissance in U.S. Oil Production, AAPG Memoir 110, pp. 167–186, 10.1306/13541961M1103589.
Sing, K.S.W., 1982. Reporting physisorption data for gas/solid systems with special reference to the determination of surface area and porosity. Pure Appl. Chem. 54 (11), 2201–2218, 10.1351/pac198254112201.
Snowdon, L.R., Brooks, P.W., Williams, G.K., Goodarzi, F., 1987. Correlation of the Canol Formation source rock with oil from norman wells. Org. Geochem. 11 (6), 529–548, 10.1016/0146-6380(87)90008-8.
Sondergeld, C.H., Rai, C.S., Curtis, M.E., 2013. Relationship between Organic Shale Microstructure and Hydrocarbon Generation. SPE Unconventional Resources Conference, The Woodlands, Texas, USA, p. 7, 10.2118/164540-MS.
Suits, N.S., Wilkin, R.T., 1998. Pyrite formation in the water column and sediments of a meromictic lake. Geology 26 (12), 1099–1102, 10.1130/0091-7613(1998)026<1099:PFITWC>2.3.CO;2.
Tassonyi, E.J., 1969. Subsurface geology, lower Mackenzie river and anderson river area, district of Mackenzie. paper 68–25 Geol. Surv. Canada 207, 10.4095/103335.
Tissot, B.P., Welte, D.H., 1984. Petroleum Formation and Occurrence. Springer-Verlag, Berlin, p. 699, 10.1007/978-3-642-87813-8.
Turner, B.W., Treanton, J.A., Slatt, R.M., 2016. The use of chemostratigraphy to refine ambiguous sequence stratigraphic correlations in marine mudrocks. An example from the Woodford Shale. Oklahoma, USA: J. Geol. Soc. 173, 854–868.
Ver Straeten, C.A., Brett, C.E., Sageman, B.B., 2011. Mudrock sequence stratigraphy: a multi-proxy (sedimentological, paleobiological and geochemical) approach. Devonian Appalachian Basin: Palaeogeogr. Palaeoclimatol. Palaeoecol. 304 (1–2), 54–73, 10.1016/j.palaeo.2010.10.010.
Wang, F., Guan, J., Feng, W., Bao, L., 2013. Evolution of Overmature Marine Shale Porosity and Implication to the Free Gas, vol. 40. Petroleum Exploration and Development, pp. 819–824. https://doi.org/10.1016/S1876-3804(13)60111-1.
Wignall, P.B., Newton, R., 1998. Pyrite framboid diameter as a measure of oxygen deficiency in ancient mudrocks. Am. J. Sci. 298, 537–552, 10.2475/ajs.298.7.537.
Williams, L.A., Crerar, D.A., 1985. Silica diagenesis; II, General mechanisms. J. Sediment. Res. 55 (3), 312–321, 10.1306/212F86B1-2B24-11D7-8648000102C1865D.
Yang, Y., Aplin, A.C., 2007. Permeability and petrophysical properties of 30 natural mudstones. J. Geophys. Res. Solid Earth 112, 1–14, 10.1029/2005JB004243.
Yang, R., He, S., Yi, J., Hu, Q., 2016. Nano-scale pore structure and fractal dimension of organic-rich Wufeng-Longmaxi shale from Jiaoshiba area, Sichuan Basin: investigations using FE-SEM, gas adsorption and helium pycnometry. Mar. Petrol. Geol. 70, 27–45, 10.1016/j.marpetgeo.2015.11.019.
Yassin, M.R., Begum, M., Dehghanpour, H., 2017. Organic shale wettability and its relationship to other petrophysical properties: a Duvernay case study. Int. J. Coal Geol. 169, 74–91, 10.1016/j.coal.2016.11.015.
Yassin, M.R., Dehghanpour, H., Begum, M., Dunn, L., 2018. Evaluation of imbibition oil recovery in the Duvernay Formation. Soc. Petrol. Eng. 21 (2), 257–272. https://doi.org/10.2118/185065-PA, 10.2118/185065-PA.
Yose, L.A., Brown, S., Davis, T.L., Eiben, T., Kompanik, G.S., Maxwell, S.R., 2001. 3-D geologic model of a fractured carbonate reservoir, Norman Wells Field, NWT, Canada. Bull. Can. Petrol. Geol. 49 (1), 86–116, 10.2113/49.1.86.